Motion-Induced Eddy Current Testing

22

Hartmut Brauer and Marek Ziolkowski

Contents

H. Brauer (✉)
Technische Universitaet Ilmenau, Ilmenau, Germany
e-mail: hartmut.brauer@tu-ilmenau.de

M. Ziolkowski
Technische Universitaet Ilmenau, Ilmenau, Germany

West Pomeranian University of Technology Szczecin, Szczecin, Poland
e-mail: marek.ziolkowski@tu-ilmenau.de; marek.ziolkowski@zut.edu.pl

N. Ida, N. Meyendorf (eds.), *Handbook of Advanced Nondestructive Evaluation*,
https://doi.org/10.1007/978-3-319-26553-7_25

Abstract

Nondestructive material testing and evaluation is a vast interdisciplinary field as well as a challenge due to the variety of applications. Whereas the focus of nondestructive testing is to identify anomalies within a specimen, the reconstruction of defect properties and their influence on the materials usability is the focus of nondestructive evaluation. In this chapter the technology of motion-induced eddy current testing (MIECT) is introduced. In contrast to traditional eddy current testing (ECT) methods, MIECT makes use of relative motion between the object under test and permanent magnets. The induced eddy currents interact with the applied magnetic field and result in a Lorentz force, depending on the impressed magnetic induction, the electrical conductivity, and the measuring velocity. Because permanent magnets produce considerably stronger magnetic fields than current-carrying ECT coils, even deep internal defects can be detected using the Lorentz force eddy current testing (LET). It is shown how the electromagnetic fields can be described theoretically and simulated numerically, as well as how imperfections/defects in non-ferromagnetic, conducting specimens can be detected using an appropriate laboratory environment. Comparative studies have shown that LET applied to metallic composite material or friction stir welds is a promising and competitive alternative to traditional ECT methods enabling the contactless evaluation of moving electrical conductors.

Introduction

Nondestructive testing (NDT) of materials and products is of great interest in a variety of modern engineering applications. NDT in general enables the initial inspection of test samples to confirm the structural integrity of safety-relevant components without causing damage.

This chapter focuses on electromagnetic NDT methods and more specifically on the motion-induced eddy current testing (MIECT). Traditional eddy current testing methods (ECT) make use of time-dependent magnetic fields to induce eddy currents in the object under test. Those are altered in the presence of physical irregularities such as flaws, cracks, or inclusions. In ECT, the variations are detected by measuring the magnetic flux through a pickup coil produced by the disturbed eddy currents in the specimen. In contrast to the ECT methods, MIECT makes use of a relative motion between the object under test and a permanent magnet configuration. The induced eddy currents interact with the applied magnetic field and result in a Lorentz force. Considering Newton's third law, the force acts on both, the specimen and the magnet itself, where it is measured. This quantity is used to evaluate the integrity of the structure under test. Thus, MIECT differs from traditional ECT methods in the way how eddy currents are induced and how signals are evaluated. It is the intent of this chapter to introduce the technology of motion-induced eddy current testing.

The Lorentz force eddy current testing (LET) method, a rather new MIECT method, was invented to complement established methods by overcoming the well-known detection limitations for subsurface defects. Originally, the MIECT

method was proposed in (Brauer and Ziolkowski 2008). Important advantages lie in the application of magnetostatic fields, which potentially allow the detection of defects lying deep inside the object under test. The working principle of LET permits the inspection of moving parts as can frequently be found in industrial settings. This necessitates appropriate NDT methods like LET, which are capable of testing moving objects. In the past more than 10 years, the authors have been conducting basic research by means of considerable funding from the German Research Foundation. This support ensures the continuous improvement of the related technologies in theory and academic practice but, so far, only allowing performance of basic research and experimental studies in university labs.

In recent years, an increase of a variety of methods can be observed which make use of relative motion between a magnetic field source producing a stationary magnetic field and the object under test. Techniques based on this principle can be classified as motion-induced eddy current testing (MIECT) methods.

The group of Chady et al. has recently realized a prototype equipment consisting of an eddy current transducer and rotating permanent magnets (Chady and Spychalski 2017). The eddy current transducer is designated for testing of planar conducting plates. A rotating head with permanent magnets is used to induce eddy currents in the specimen. Two Hall-effect devices connected in a differential manner are utilized to measure the eddy current reaction. This inspection system is effective especially in cases of thick metallic elements, when it is necessary to utilize low excitation frequency, or in systems without power supply. Thus, the system is suitable for applications where it is important to achieve high penetration depth.

The group of Ribeiro and Ramos proposed in 2013 with the velocity-induced eddy current testing (VIECT) another approach where the magnetic fields are also measured (Geirinhas Ramos et al. 2013). Ramos et al. investigated the applicability of moving stationary magnetic field sources using DC coils in the framework of NDT (Ramos et al. 2013; Rocha 2017). They measured the disturbances of the magnetic field resulting from a defect directly by means of giant magneto-resistive (GMR) sensors.

Moreover, they also exchanged the magnetic field source with a permanent magnet in order to achieve higher flux densities and an increased induced eddy current density inside the moving specimen. The sensor orientation has to be chosen carefully when using GMR sensors in order to avoid saturation effects. This can be overcome by applying differential coils as magnetic field sensors as it is also done in the framework of ECT. In this way, only the temporal change of the magnetic flux resulting from a passing defect is measured. Rocha et al. extended the analysis to the application of Hall sensors instead of GMRs and pickup coils (Rocha et al. 2015b). They also investigated the defect response signals for different permanent magnet configurations and proposed the use of sensor arrays to expedite the assessment of larger areas. In a subsequent study, the application of GMRs, differential coils, and Hall sensors was compared in the framework of MIECT (Rocha et al. 2015a). As a result, it turned out that GMRs were able to detect defects when crossing the edges of the defect. In contrast, pickup coils and Hall sensors also provided signals when the probe passed the defect in its centerline.

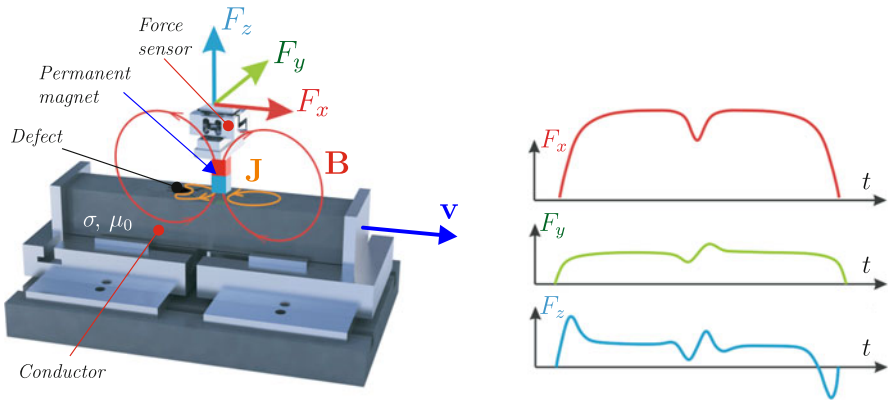

Fig. 1 Lorentz force eddy current testing for contactless evaluation of electrically conducting materials

In 2015, another MIECT technique was proposed in (Tan et al. 2015). In contrast to previous studies which made use of translational motion, they proposed a system using rotational motion of the magnetic field source to induce eddy currents inside the object under test. A diametral magnetized, cylindrical permanent magnet rotates in close vicinity of a conductive object, and anomalies are analyzed by means of the variations in the electromagnetic torque. The use of rotational motion provides the opportunity to design portable MIECT systems in line with ECT devices currently available.

The presented studies are all limited to the analysis of surface-breaking defects indicating the early state of MIECT systems. However, it is emphasized that MIECT is not restricted to detect flaws on the surface. As in (Brauer and Ziolkowski 2008) is shown, the MIECT system consisting of a permanent magnet combined with a force sensor can be used to detect defects in conducting, nonmagnetic specimen. The principal setup is shown in Fig. 1. Because the Lorentz forces are measured, this method has been called Lorentz force eddy current testing (LET) (Brauer et al. 2014).

Lorentz Force Eddy Current Testing (LET)

Lorentz force eddy current testing (LET) belongs to the group of MIECT-type methods. It is a technique for nondestructive and contactless evaluation of electrically conducting specimens. The basic principle, shown in Fig. 2, is based on the interaction between a permanent magnet and a moving specimen. As a consequence of this motion, eddy currents are induced inside the object under test, which in turn react with the magnetic field, producing a Lorentz force acting on both, the specimen and the permanent magnet. The novelty of the method lies in the determination of the measurement signal. In contrast to ECT and other MIECT techniques, the force

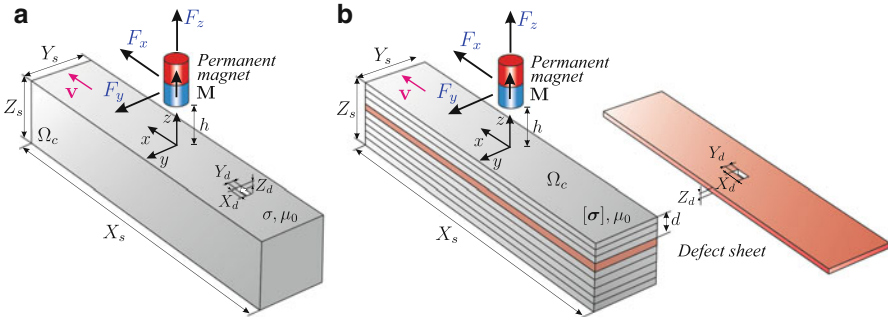

Fig. 2 General principle of Lorentz force eddy current testing for contactless evaluation of electrically conducting material. The specimens and the geometrical parameters of the LET problem under investigation are shown in (**a**) for solids and in (**b**) for layered structures

acting on the magnet is measured using force sensors. In the presence of a defect, the eddy current profile and, hence, the resulting Lorentz force are perturbed. The physical principle of LET is an analogy to Lorentz force velocimetry (LFV) (Thess et al. 2006). In LFV, the main goal is to determine the flow rate of a conducting liquid by means of the Lorentz force which is proportional to the velocity of the liquid (Thess et al. 2007).

LET was initially demonstrated as an alternative NDT method in (Brauer and Ziolkowski 2008). The same authors in (Ziolkowski and Brauer 2010) tackled the numerical analysis of the reported experimental setup and proposed techniques to analyze the electromagnetic field problem with increased computational efficiency. The work on LET in an experimental and numerical framework was continued by Uhlig and Zec (Uhlig 2014; Zec et al. 2013).

A very important study is related to the investigation of the effect of defect depth on the Lorentz force signals exerting on the magnet. To study the impact of the defect depth, a layered specimen containing a number of aluminum sheets of the same thickness (usually 2 mm) was used. The defect depth can be changed easily if the position of the layer containing the defect is modified (Fig. 2).

A demonstrative model of LET is proposed and investigated in (Uhlig et al. 2012a). It consists of a modification to the well-known creeping magnet experiment, where a permanent magnet is slowly falling down a copper pipe (Donoso et al. 2011). The modification in this study consists of adding defects into the pipe wall such that the eddy current distribution and Lorentz force profile are disturbed. The LET method is extended to the determination of the electrical conductivity of the specimen assuming that the object under test is free of defects (Uhlig et al. 2012b). This technique is called Lorentz force sigmometry (LoFoS). It is shown that the lift-to-drag ratio of the Lorentz force components is proportional to the conductivity of the specimen such that $\sigma = \alpha F_z/F_x$ with a calibration factor α which is determined experimentally. Besides the mentioned investigations, fundamental studies exist on the influence of the Lorentz force on geometrical parameters such as the lift-off distance, the size of the magnet, as well as the size and depth of the defect (Uhlig

et al. 2011; Zec et al. 2014). These studies were accomplished by analyzing how the velocity or conductivity affects the resulting Lorentz force profile.

The state of the art of LET has been summarized in (Brauer et al. 2014). It includes a summary of the experimental setup, the numerical modeling techniques, and currently the applied defect reconstruction methods. The investigations on the forward models were supported in (Petković et al. 2013), addressing the inverse problem, i.e., the identification of the defect called Lorentz force evaluation (LFE). They proposed reconstruction algorithms to determine the shape and the location of the defects solely out of the Lorentz force profiles. There were following up several studies of the LFE problem, i.e., considering the defect identification as an extension and improvement of this first approach (Mengelkamp et al. 2015, 2016, 2017; Petković et al. 2013).

Theory

Nondestructive testing (NDT) and nondestructive evaluation (NDE) of electrically conductive objects require reliable methods to detect material anomalies or deep-lying defects. Besides radiographic, ultrasonic, or optical techniques, electromagnetic methods such as eddy current testing (ECT) find a wide range of applications due to low-cost, easy-to-use equipment and low demands on the measurement environment (Hellier 2013; Jiles 1990). However, one of the most limiting factors in ECT is the frequency-dependent skin depth (Brauer and Ziolkowski 2008). This restricts the capability to detect deep-lying defects. With Lorentz force eddy current testing (LET), a novel electromagnetic nondestructive testing technique is presented (Thess et al. 2006; Uhlig et al. 2012a, b; Zec et al. 2013) with the aim to overcome this limitation. Lorentz force eddy current testing is based on setting an electrically conductive specimen into relative motion to a constant magnetic field. Due to Ohm's law for moving conductors, eddy currents are induced in the conductor under test

$$\mathbf{J} = \sigma\left(-\frac{\partial \mathbf{A}}{\partial t} - \nabla\varphi + \mathbf{v} \times \mathbf{B}\right) \tag{1}$$

where $\mathbf{J}$ denotes the induced current density, φ the scalar electric potential, $\mathbf{A}$ the magnetic vector potential ($\mathbf{B} = \nabla \times \mathbf{A}, \nabla \cdot \mathbf{A} = 0$), $\mathbf{v}$ the conductor velocity, and $\mathbf{B}$ the total magnetic flux density. $\mathbf{B}$ can be divided into a primary magnetic field (caused by a permanent magnet) and a secondary magnetic field generated by the eddy currents. The interaction of the constant magnetic field and the induced eddy currents results in a Lorentz force $\mathbf{F}^{(L)}$ acting on the specimen. Due to Newton's third law, an equal force $\mathbf{F}^{(PM)}$ is exerted on the permanent magnet in the opposite direction

$$\mathbf{F}^{(PM)} = -\mathbf{F}^{(L)} = \int_{V_c} \mathbf{J} \times \mathbf{B}\, \mathrm{d}V \tag{2}$$

with V_c describing the volume of the specimen. If a defect is present in the conductive material, perturbations in the measured Lorentz force occur. Based on these perturbations, the defect can be detected and perhaps reconstructed.

In contrast to LET, common eddy current testing uses a time-changing current in a primary coil which generates a time-changing primary magnetic field $\mathbf{B}^{(p)}$. Usually, the signal used to evaluate the material is the change in impedance of the secondary coil.

Both principles are based on the induction of eddy currents, whereas major differences arise in shape and magnitude of the induced current densities as well as in the method of signal evaluation. Figure 3 shows a comparison of the two methods and illustrates the perturbation of eddy currents due to defects. In both methods, a secondary magnetic field $\mathbf{B}^{(s)}$ is generated which interacts with the primary magnetic field $\mathbf{B}^{(p)}$. The total magnetic field is given by the sum of the two fields:

$$\mathbf{B} = \mathbf{B}^{(p)} + \mathbf{B}^{(s)}.$$

The formalism to describe the LET and ECT problem in theory is given by the magnetic convection diffusion equation (Zec 2013; Zec et al. 2013), which can be written in its potential form as

$$\nabla \times \left(\frac{1}{\mu_0} \nabla \times \mathbf{A} - \mathbf{M} \right) = -\sigma \left(\frac{\partial \mathbf{A}}{\partial t} + \nabla \varphi - \mathbf{v} \times \nabla \times \mathbf{A} \right) + \mathbf{J}^{(e)}, \tag{3}$$

if a linear and non-ferromagnetic material was assumed. In (3), $\mathbf{M}$ denotes the magnetization vector, $\mathbf{J}^{(e)}$ the external current density, and $\mathbf{v}$ the velocity of the object under test. The limiting factor of ECT is the skin depth $\delta = \sqrt{2/\omega\sigma\mu_0}$, which results in a fast decay of the information signal for subsurface defects.

A similar factor, namely, the magnetic Reynolds number R_m, can be defined for moving conductors. By transforming the magnetic convection diffusion equation into its nondimensional form, the Reynolds number can be derived (Uhlig et al. 2012a):

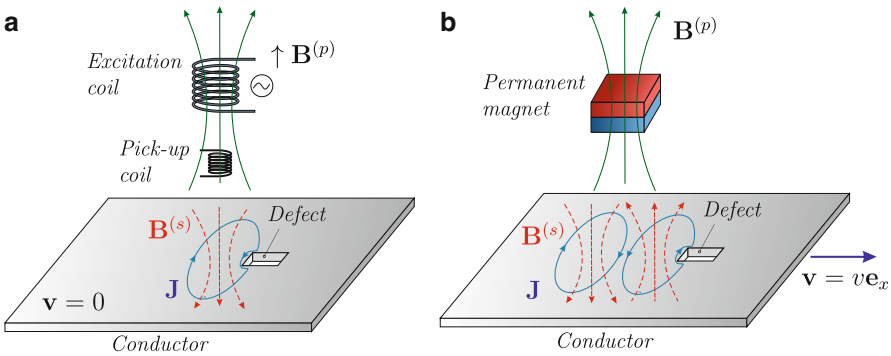

Fig. 3 Comparison of characteristic eddy current profiles observed in ECT and LET: (**a**) in ECT, the eddy currents show a circular profile, which are similar to an imprint of the primary excitation coil; (**b**) in LET, the eddy currents follow a figure of eight and do cross below the magnet

$$R_m = \mu\sigma \mid \mathbf{v} \mid L. \tag{4}$$

The parameter L is the typical length scale of the problem. In general, for $R_m \ll 1$ diffusion of the magnetic field dominates, and the resulting field is primarily determined by the boundary conditions and the primary magnetic field $\mathbf{B}^{(p)}$. For $R_m \gg 1$, the magnetic field lines are deformed in the moving direction, which results in a similar phenomenon as the skin effect.

Comparison of ECT and LET

A comparison between the ECT technique and LET is reported in (Carlstedt et al. 2013, 2014). In order to compare both methods from the numerical point of view, a detailed model of the applied ECT sensor is necessary. The probe under investigation was a differential-type probe PKA-48 (Rohmann GmbH), including secondary pickup coils. It was used with the ECT device Elotest N300 (Rohmann GmbH). Knowing the inner structure of the commercial ECT probe, finite-element models of both probes have been defined and used for the numerical comparison. First this analysis enabled the possibility to compare the defect response signals obtained experimentally with numerical simulations (Porzig et al. 2014). An example of 3-D FEM simulations is shown in Fig. 4.

Using the $\mathbf{A} - \varphi$ potential formulation, the LET field problem can be described by (3), but without the external current density on the right-hand side. This formulation separates the two induction phenomena into the moving part $\mathbf{v} \times \mathbf{B}$ and the time-changing part on the right-hand side. Depending on the definition of the frame of reference, two equivalent types of the general magnetic field induction equation can be distinguished (Zec 2013; Zec et al. 2013). In the so-called moving frame of reference, the global coordinate system is associated with the moving permanent magnet, i.e., the conducting object moves in the direction along the x-axis with velocity v. If the conducting object moves with a constant velocity and has a constant cross section normal to the direction of motion, e.g., the object is free of defects, the time derivative $\partial A/\partial t$ vanishes and (3) is reduced to a quasi-static approach.

The major differences between ECT and LET are given by the shape and the magnitude of the induced eddy current profile as well as by the evaluated signal. The impedance variations of the imaginary part ΔZ_i and the back-induced voltage U_2 in the secondary pickup coil from ECT have been compared to the force perturbations

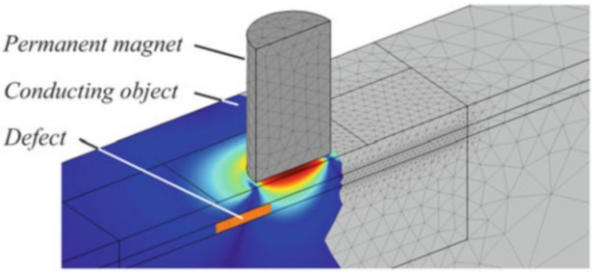

Fig. 4 3-D FEM model used for LET simulations

in the case of LET (Carlstedt et al. 2014). The normalized force perturbations (LET) and impedance perturbations (ECT) representing the normalized defect response signals one will get from both methods are shown in Fig. 5. The graph shows normalized signals of the drag force F_x together with the imaginary part of the secondary coil impedance at comparable source dimensions.

Usually, the ECT method is applied in stationary applications. However, when the object under test is moving relative to the ECT probe, the induced voltage in the pickup coil is modulated in the defect region. This effect is shown in Fig. 6.

If the velocity-to-frequency ratio v/f increases, the amount of sinusoidal periods in the defect region decreases. It is shown in (Carlstedt et al. 2014) that the use of the Hilbert transform of the secondary induced voltage $\mathcal{H}\,[U_2(t)]$ is suitable to post-process the modulated defect response signals to determine the envelope of the modulated signal. In practice, this requires additional adjustments of currently available ECT devices. A direct comparison between both methods in terms of defect depth and velocity showed that with ECT, it was possible to detect defects of size $[X_d, Y_d, Z_d] = [12\text{ mm}, 2\text{ mm}, 2\text{ mm}]$ up to a depth of 6 mm at a velocity of $v = 0.25$ m/s considering a frequency of $f = 100$ Hz. In contrast, the LET method was able to resolve the defect up to a depth of 8 mm at $v = 0.5$ m/s.

In many experiments, it was observed that the detection of subsurface defects in stacked aluminum sheets is possible for both testing techniques using the described experimental setup (Carlstedt et al. 2013). In the ECT method, the detection of a subsurface defect is mainly limited by the frequency-dependent penetration depth, i.e., if deep internal defects should be detected, the testing frequency has to be as low as possible. On the other hand, if low frequencies are used, the performance of the electronic amplifier becomes more important due to the weak signals. Furthermore, the testing speed is strongly restricted depending on the properties of defects, e.g., characteristic length and shape. In LET, a relative movement between the permanent magnet and the specimen is required to induce eddy currents. To create a sufficiently

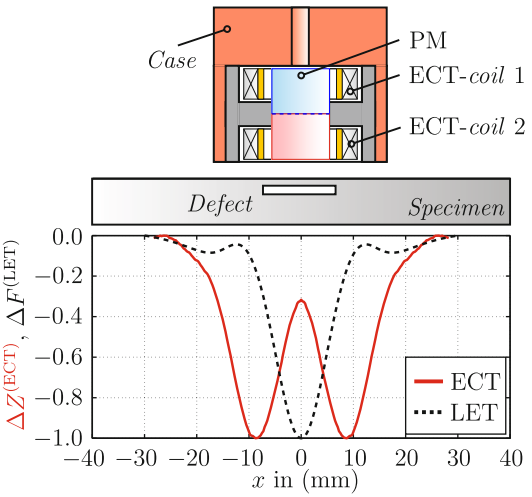

Fig. 5 Normalized defect response signals in the case of ECT and LET assuming equivalent dimensions (Carlstedt et al. 2013)

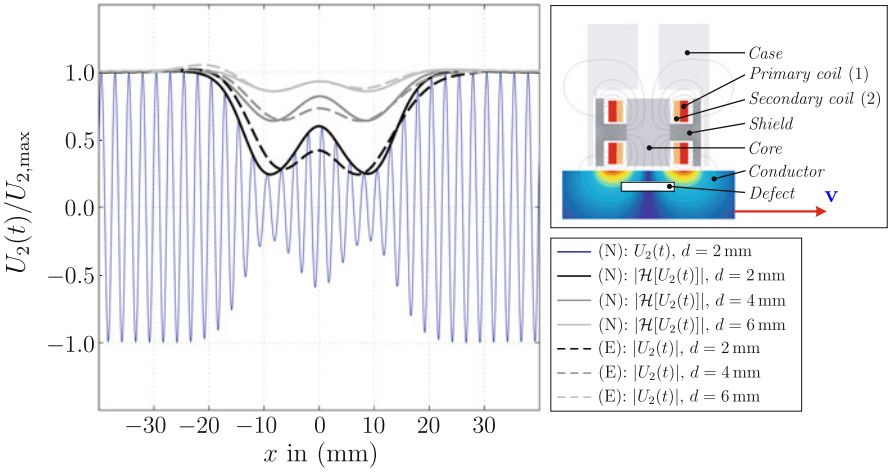

Fig. 6 Modulated secondary induced voltage $U_2(t)$ in the pickup coils in the case of moving objects under test ($v = 0.25$ m/s, $\sigma_0 = 30.61$MS/m) (Carlstedt et al. 2014)

large Lorentz force, the relative velocity has to be high enough to detect small perturbations induced by subsurface defects. With the increasing speed, the absolute force and the force perturbations increase linearly at magnetic Reynolds number $R_m < 1$.

It can be concluded that both methods possess individual advantages. The classical ECT method is suitable to inspect stationary objects, which is not possible with LET or any other MIECT-type method. However, if the object is in motion, the use of alternating currents can be omitted. In this way, it is possible to apply permanent magnets, which produce considerably higher magnetic flux densities compared to current-carrying coils. Therefore, the magnitude of the desired force signal is theoretically adjustable with the velocity for optimal utilization of the applied force sensor. In practice, the force sensor is sensitive to unwanted vibrations of the environment and the system itself.

To summarize, both testing techniques are highly dependent on the used sensors and measurement electronics as well as on the available testing speed. Consequently, many areas of application of LET and ECT, respectively, will be different. Comparative studies (Carlstedt et al. 2013, 2014) showed that LET is a promising and competitive alternative to traditional ECT methods considering the contactless evaluation of moving electrical conductors.

Motion-Induced Eddy Current Testing (MIECT)

Numerical Simulations

The intrinsic phenomena associated with electric and magnetic fields affect almost all aspects of our everyday life. This is accompanied by continuous development and design of more sophisticated electromechanical devices, which result in better

functionality, higher efficiency, and increased safety. Depending on the particular application, this task strongly relies on the accurate modeling of the electromagnetic fields within the device. Apart from providing exact and fast solutions, a closed-form analytical expression helps in better understanding of the underlying physical phenomena associated with the problem under investigation. Unfortunately, these solutions are not always available, and they can be obtained only for some simplified device and field configurations. Thus, in NDT&E applications, the development and optimization of various testing techniques are performed using numerical methods (Ida 1995). Due to its ability to handle complex geometries, anisotropic and inhomogeneous material properties, a widely used numerical method in NDT&E applications, are the finite element method (FEM) (Ida and Bastos 1997). In general, analysis of LET systems requires accurate and time-efficient numerical approaches to allow either extensive scans of an object under test or parametric and optimization studies. For the implementation of the proposed approaches, the commercial software package COMSOL Multiphysics (COMSOL 2018) has been used.

Computation of Eddy Current Distributions in Moving Parts

The LET belongs to a special class of electromagnetic field phenomena in which various effects caused by parts set in a relative motion occur. These effects represent the basic operating principle over a wide range of electromechanical devices in different application areas such as electrical machines, magnetic levitation systems, inductive heating, eddy current brakes, nondestructive testing and evaluation (NDT&E), etc. Due to its tremendous industrial relevance, the application of FEM to this particular type of field problems, also known as the moving eddy current problems, has undergone extensive research over the past decades (Ying et al. 2007).

In principle, independently of the actual type of motion (translation or rotation), all existing techniques for simulation of general moving eddy current problems can be classified into (i) fixed grid methods and (ii) moving or time-changing grid methods (Demenko 1996).

The fixed grid methods are usually applied to 2-D/3-D static or time-harmonic eddy current problems involving uniformly moving conducting parts having invariant cross section in the motion direction (Binns et al. 1992; Bird and Lipo 2009; Demenko 1996; Rodger and Eastham 1985; Rodger et al. 1990, 1991; Ying et al. 2007; Ziolkowski and Brauer 2010). The field problem is formulated in the moving frame of reference where the additional velocity term $(\mathbf{v} \times \nabla \times \mathbf{A})$ is used to describe the contribution of the induced eddy currents within the moving electrically conducting part. This approach, also referred to as the quasi-static approach (QSA) (Ziolkowski and Brauer 2010), is very efficient in terms of computational time since only one stationary analysis needs to be performed to obtain an accurate steady-state solution. For some simple device configurations, several authors combine FEM with analytical solutions as well (Bird and Lipo 2009; Kirpo et al. 2011) and report a considerable reduction of the simulation time and increased accuracy. However, apart from simple geometries, the analysis is restricted to stationary and time-harmonic problems.

The moving grid methods are more general, and they can be applied to simulate a wide variety of electromechanical devices involving linear or rotational movement. In principle, from the model topology point of view, all available techniques are quite similar. The main idea is to decompose the whole computational domain into two parts associating them with the moving or with the fixed part of the assembly (Demenko 1996; Trowbridge and Sykulski 2006; Ying et al. 2007). Within each part, the governing equations are solved in their own frame of references, whereas the relative displacement and the field coupling are provided on the introduced interface (Biddlecombe et al. 1998; Davat et al. 1985). Depending on the actual interface, which can have constant or variable lift-off distance, to achieve the coupling, many different techniques have been applied.

One of the most widely applied moving grid methods to model relative displacements in general eddy current problems is the so-called sliding mesh technique (SMT) (Buffa et al. 2000). Similarly to all other methods, SMT, also referred to as the moving mesh method (Ying et al. 2007) or slip surface method (Preston et al. 1988), requires two independent meshes to be defined. To provide the relative displacement, the meshes are simply slid relatively to each other eliminating any need to alter their structure. The governing equations are solved independently in the fixed reference frame of each moving part, thereby avoiding the convection (velocity) terms. Depending on the mesh distribution along the introduced interface, which can be conforming or nonconforming, the field continuity can be preserved using several coupling techniques. In the case of conforming meshes, the unknown potentials on each side of the sliding interface are made equal in the same way as Dirichlet boundary conditions are imposed (Muramatsu et al. 1996, 1999; Preston et al. 1988; Yamazaki 1997, 1999; Ying et al. 2007). However, the displacement is strictly controlled by the size of the finite elements in the motion direction and the time-step size of the transient solver. To overcome this limitation, nonconforming meshes along with Lagrange multipliers have been introduced (Rodger et al. 1990). The Lagrange multiplier approach introduces an additional set of variables on the sliding interface which ensures the continuity of the field in a weak sense (Golovanov et al. 1998; Lai et al. 1991; Leonard et al. 1993; Marechal et al. 1992). Unfortunately, the existence of additional variables considerably deteriorates the conditioning of the stiffness matrix (Antunes et al. 2006a, b; Golovanov et al. 1998).

Numerical Modeling

The main aim of this section is to introduce a new FEM-based methodology, which can be used to analyze and develop future LET systems. The particular emphasis is placed on the reduction of the overall computational requirements while maintaining the accuracy of the solution. Additional goals include development of simplified numerical models which enable fast 2-D and 3-D LET analysis in conjunction with the verification of assumed simplifications. The problem is simplified step-by-step, starting from time-dependent approaches, applying quasi-static approximations, and assuming a weak reaction from the conductor. For comparison and verifications of

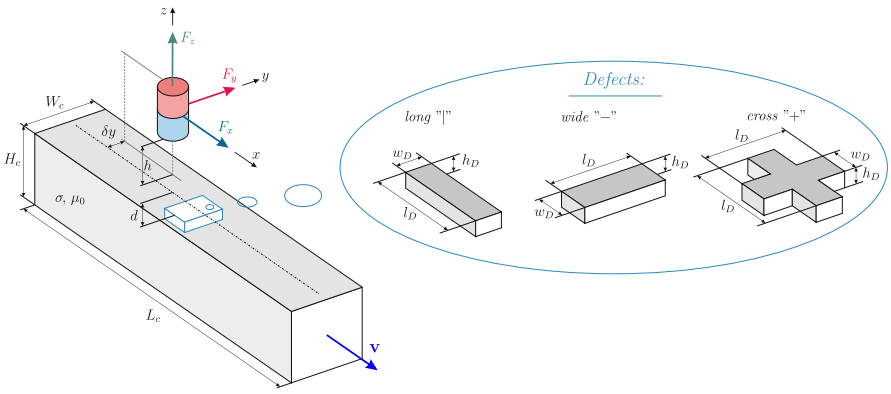

Fig. 7 Definition of the LET benchmark problem. The conductor contains three types of defects: long ("|"), wide ("−"), and cross ("+")

different approaches, a benchmark problem which represents a typical LET configuration has been considered.

Benchmark Problem

As a LET benchmark problem, a generic conductor with pre-defined artificial defects, moving across the static magnetic field, is chosen (Fig. 7). The conductor under test is considered to be nonmagnetic with the electrical conductivity denoted by σ and magnetic permeability equal to the permeability of vacuum $\mu = \mu_0$. It has a rectangular cross section determined by its width W_c and height H_c, whereas its length is denoted by L_c. A cylindrical permanent magnet described by magnetization $\mathbf{M}$ is used as a source of the static (primary) magnetic field. The diameter and the height of the magnet are denoted by D_m and H_m, respectively. The magnet is placed centrally above the conductor under test ($\delta y = 0$) at a lift-off distance h.

For the analysis, three different types of artificial defects, namely, long ("|"), wide ("−"), and cross ("+"), have been considered. Defects are placed centrally within the conductor at depth d below its surface. They are characterized by their width w_D, height h_D, and length l_D. The conductivity of the defect is denoted by σ_d. In order to reduce the number of dependent variables, the magnetic Reynolds number (R_m) has been used for the analysis (4). It involves the characteristic length-scale parameter L whose definition depends on the particular problem at hand and characterizes the moving conductor.

Logical Expression Approaches

The main idea of the logical expression approaches (LEA) that allows fast computations of 2-D/3-D eddy current problems including parts in relative motion is presented (Zec et al. 2013). Using the proposed methodology, the spatial coordinates of moving parts, either conducting or nonconducting, are modeled on a fixed computational grid using logical expressions (LE). By applying the principles of Boolean algebra directly in finite element analysis (FEA), the shape of moving parts is determined on the fly by calculating the constraints given by LE and filtering the

finite elements in those domains where LE are introduced. Figure 8 shows three basic geometrical primitives, i.e., box, cylinder, and sphere, which are modeled using LE. Independent to the type of reference frame used in LET analysis, modeling of moving parts using LE requires the existence of a homogeneous zone in which these expressions are applied. This zone is referred to as the moving domain, and it is determined by the shape of the moving part and its relative displacement L (Fig. 8). In order to introduce the motion and to determine the shape of moving parts, the constraints given by LE are defined as time dependent. This step represents the basic idea of the logical expression approach (Zec et al. 2013).

Depending on the definition of the global frame of reference, the LET analysis has been performed using two different implementations of LEA:

1. In the case of fixed frame of reference, the logical expressions are used to model the motion of the permanent magnet.
2. In the case of moving frame reference, the logical expressions are used to model the relative motion of the defect.

These two specific LEA implementations are referred to as the moving magnet approach (MMA) and the moving defect approach (MDA), respectively.

Moving Magnet Approach

In the implementation of the moving magnet approach (MMA), the global coordinate system is associated with the conducting object (fixed frame of reference), and the logical expressions are used to describe the motion of the used cylindrical permanent magnet (Fig. 9). The magnet is moving with constant velocity v along the model x-axis in close vicinity of the conductor containing an artificial defect below its surface. The moving domain is defined in the surrounding air region. The cross section of the moving domain is determined by the height H_m and the diameter D_m of the magnet, while its length depends on the starting position X_{start} and its relative displacement L. In general, the starting position X_{start} is the distance of the moving object to the origin of the coordinate system at $t = 0$. It has to be large

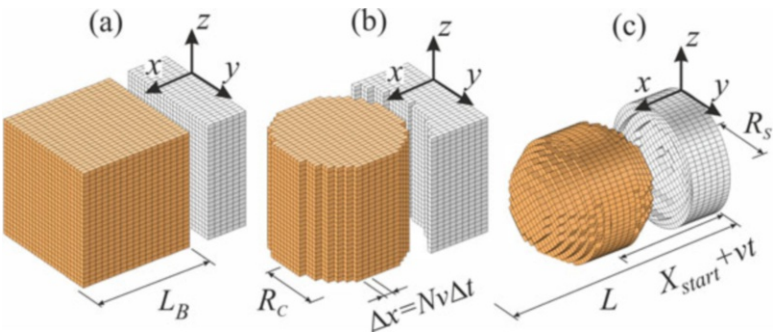

Fig. 8 Basic geometric primitives defined by logical expressions: (**a**) box, (**b**) cylinder, and (**c**) sphere

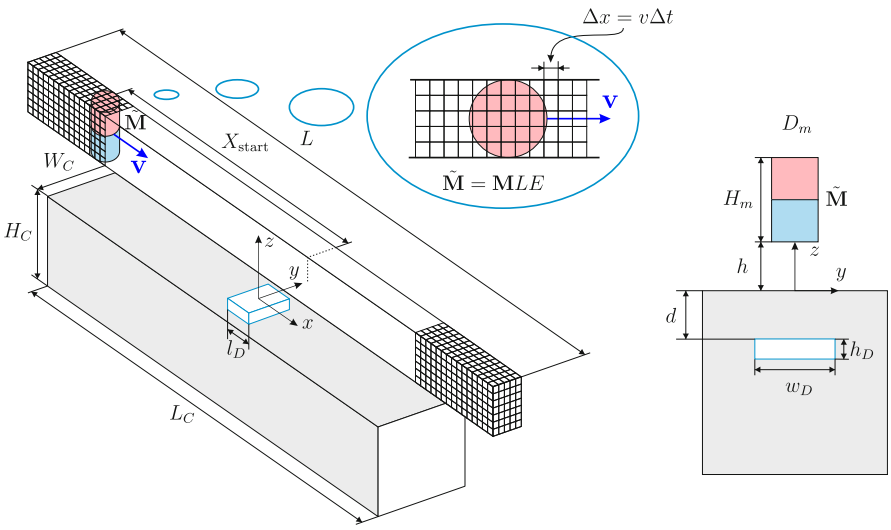

Fig. 9 Implementation of the moving magnet approach (MMA). The moving domain is defined in the air region

enough to avoid any influence of the used initial conditions on the resulting Lorentz force perturbations. Applying the modified vector potential $\mathbf{A}^*$ (Zec 2013), the governing system of equations in MMA is given by:

$$\nabla \times \left(\frac{1}{\mu_0} \nabla \times \mathbf{A}^* - \mathbf{M} \right) = -[\boldsymbol{\sigma}] \frac{\partial \mathbf{A}^*}{\partial t} \tag{5}$$

$$\nabla \cdot \left(-[\boldsymbol{\sigma}] \frac{\partial \mathbf{A}^*}{\partial t} \right) = 0 \tag{6}$$

where $[\boldsymbol{\sigma}]$ is a diagonal tensor of electrical conductivity $[\boldsymbol{\sigma}] = \mathrm{diag}(\boldsymbol{\sigma}_{xx}, \boldsymbol{\sigma}_{yy}, \boldsymbol{\sigma}_{zz})$. This requires both nodal and edge finite element formulations in single computational domain. Due to the fact that (5) and (6) do not introduce the additional velocity term, the resulting system of equations remains symmetric. Another important feature of MMA is that the stiffness matrix has to be assembled only once during the entire motion of the magnet which additionally reduces the total computational time. This is because the motion is provided by simple modification of the magnetization vector $\mathbf{M}$ which appears as a source term in the resulting FEM formulation.

Moving Defect Approach

In the moving defect approach (MDA), the global coordinate system is assigned to the permanent magnet (moving frame of reference). In this reference frame, the magnet is stationary, and the conductor is moving in opposite direction with velocity $-v$. For the given LET problem, the use of LE to describe the motion of the whole conducting domain would be computationally very expensive. However, the implementation of LEA in the

moving reference frame can be considerably simplified if only perturbations of Lorentz force caused by defects are required, which is in fact a typical LET problem. Thus, it is sufficient to model only the movement of the defect relatively to the magnet, instead of modeling the motion of the whole conductor.

In MDA the moving domain is defined entirely inside the conductor where LE are used to model the motion of the particular defect (Zec et al. 2013). The shape and position of the moving domain are defined by the cross section of the defect $w_D \times h_D$, its relative displacement L, and depth d. Similar to the previous MMA, applying the modified vector potential $\mathbf{A}^*$ in MDA results in the system of governing equations given by:

$$\nabla \times \left(\frac{1}{\mu_0} \nabla \times \mathbf{A}^* - \mathbf{M} \right) = [\boldsymbol{\sigma}] \left(-\frac{\partial \mathbf{A}^*}{\partial t} + \mathbf{v} + \nabla \times \mathbf{A}^* \right) \tag{7}$$

$$\nabla \cdot \left[[\boldsymbol{\sigma}] \left(-\frac{\partial \mathbf{A}^*}{\partial t} + \mathbf{v} \times \nabla \times \mathbf{A}^* \right) \right] = 0 \tag{8}$$

This requires both nodal and edge finite element formulations to be applied in the computational domain. In contrast to MMA, the formulation used in MDA involves the additional velocity term which makes the resulting system of equations non-symmetric. Additionally, the modification of the electrical conductivity by time-dependent LE, introduced by MDA, modifies the resulting stiffness matrix as well. Therefore, the stiffness matrix has to be reassembled at every time step which increases the computational time compared to MMA.

Quasi-static Approach

The moving magnet approach (MMA) and the moving defect approach (MDA) assume no simplifications for the given LET analysis. They offer accurate results for any relative testing velocity $\mathbf{v}$ between the magnet system and the conductor and for any material and geometry parameters involved. Thus, they are valid for finite values of the magnetic Reynolds number, whether the conductor contains material defects or not. If the LET configuration under investigation is time independent, i.e., it involves uniformly moving conductors with a constant cross section normal to the direction of motion (conductors free of defects), the analysis can be considerably simplified. A single stationary analysis can be performed to obtain an accurate steady-state solution, e.g., the Lorentz force acting on the magnet system. This assumption requires the moving frame of reference, where the additional velocity term ($\mathbf{v} \times \nabla \times \mathbf{A}$) is used as a source of the induced eddy currents inside the conductor in uniform motion

$$\nabla \times \left(\frac{1}{\mu_0} \nabla \times \mathbf{A} - \mathbf{M} \right) = [\boldsymbol{\sigma}](-\nabla \varphi + \mathbf{v} + \nabla \times \mathbf{A}) \tag{9}$$

$$\nabla \cdot [[\boldsymbol{\sigma}](-\nabla \varphi + \mathbf{v} + \nabla \times \mathbf{A})] = 0. \tag{10}$$

The second equation results from the current conservation law $\nabla \cdot \mathbf{J} = 0$, and it is an additional equation for the electric scalar potential φ. This system of equations

takes the deformation of the magnetic field lines correctly into account making it valid for any value of the R_m. Although (9) and (10) provide fully correct solutions only for conductors without any material defects, their use can be still extended to NDT applications as well. It has been shown that for LET systems resulting in small R_m, they can be used for fast Lorentz force calculations on the moving magnet even for conductors with defects (Ziolkowski and Brauer 2010). The method is referred to as a quasi-static approach (QSA). As a direct consequence of low magnetic Reynolds numbers ($R_m < 1$), the diffusion time of the magnetic field into the conducting object was estimated as $\tau \sim R_m \cdot L/v$, where L is the characteristic length scale of the conductor. This basically justifies the instantaneous field reaction ($\partial \mathbf{B}/\partial t \rightarrow \mathbf{0}$) to any perturbation of induced currents, which is assumed in QSA. Nevertheless, if this is not the case, the full transient form of (9) and (10) has to be considered, representing the governing equation of already presented moving defect approach (MDA). In the implementation of QSA, only the change in relative position between the magnet and the defect must be provided. This is done either by moving the magnet system relative to the defect or vice versa (Ziolkowski and Brauer 2010). In any case, this requires a time-consuming re-meshing procedure of the entire model geometry for each new configuration. The re-meshing of the geometry can be avoided if the basic principle of the logical expression approach (LEA) is combined with the quasi-static formulation given by (9) and (10). In this LEA implementation, the time variable used in different LE is just a parameter which needs to be changed from one stationary solution to another providing the displacement of the moving part (magnet or defect). This means that the same geometry used for the implementation of the LEA can be used for implementation of QSA as well. The only difference introduced by QSA is in the governing equation in the conducting region, which is now in its stationary form and contains an additional scalar potential φ. In regions free of eddy currents (surrounding air region and permanent magnet), the magnetic scalar potential is used.

Weak Reaction Approach

The induction problem at hand can be further simplified in the case of low magnetic Reynolds numbers ($R_m \ll 1$). In this case, the induced eddy current density is so small that its magnetic field $\mathbf{B}^{(s)}$ is vanishingly small compared to the primary magnetic field $\mathbf{B}^{(p)}$ of the magnet system. By setting $\mathbf{B}^{(s)} = 0$, the magnetic and electric fields are decoupled and, therefore, can be treated independently. Hereinafter, this effect will be referred to as a *weak reaction* by the conductor to the magnetic field. Special attention must be paid to the emerging Lorentz forces when using weak reaction-based approaches. By neglecting the secondary magnetic field, the spatial symmetry of the electric and magnetic field is enforced. As a consequence, the lift component of the Lorentz force vanishes if the conductor is free of defects and if the magnet is far from any outer edge of the conductor, such that $F_z^{(0)} = 0$. However, in the presence of defects, the symmetry of the fields no longer holds, and the defect response signal ΔF can be determined.

Comparison of Numerical Approaches

The approaches discussed above differ in their treatment of the secondary magnetic field $\mathbf{B}^{(s)}$. Hence, it is necessary to investigate their applicability in terms of magnetic Reynolds number R_m. The ratio between primary and secondary magnetic fields depends on the underlying geometry of the problem, as indicated by the characteristic length L in R_m. To conduct an expressive comparison, an exemplary LET problem that corresponds to the dimensions of the available laboratory setup is defined (Zec 2013).

The absolute defect response signal (ADRS) $\Delta\mathbf{F}$ is defined as the force perturbation resulting from a defect. Because Lorentz forces are also present in the unperturbed case, the ADRS can be mathematically defined by the difference between the perturbed force profile $\mathbf{F}$ and unperturbed force profile $\mathbf{F}^{(0)}$:

$$\Delta\mathbf{F} = \mathbf{F} - \mathbf{F}^{(0)}. \tag{11}$$

Thus, the ADRSs are calculated for different magnetic Reynolds numbers R_m by varying the velocity.

No significant differences can be identified between time-dependent approaches and WRA, which indicates that time-dependent effects are negligible. When increasing R_m, secondary fields and time-dependent effects become prevalent, resulting in nonsymmetric field and force profiles. The ADRS obtained using WRA retains its symmetry because the secondary fields are neglected. Consequently, WRA overestimates the ADRS amplitude compared to time-dependent approaches in the case of high R_m. The ADRS obtained using QSA is closer to ADRS values obtained using MDA and MMA, because it includes the stationary part of the secondary magnetic field ($\mathbf{B}^{(s)} \neq 0$). In the case of high R_m, the time-dependent part of the secondary magnetic field $\partial\mathbf{B}^{(s)}/\partial t$ has an increasing influence on the ADRS. By comparing the results of QSA to those of MDA and MMA, a delayed and damped force response can be seen. As expected, the solutions from MMA and MDA are equivalent and yield very similar force profiles, because they only differ in the definition of the frame of reference. These effects pertain to both isotropic and anisotropic specimens. However, the ADRS has higher amplitudes in the anisotropic case than in the isotropic case. This phenomenon can be explained based on the imposed condition that $J_z = 0$ because $\sigma_{zz} = 0$. As a consequence, the current flows around the defect only in the $x - y$ - plane (i.e., not vertically). This phenomenon positively influences the resulting Lorentz force in terms of the ADRS amplitude. The shape of the ADRS is weakly influenced by this condition because in the unperturbed case, the induced eddy currents already flow solely in the $x - y$ - plane. However, some differences between the two cases can be identified. Their anisotropic profiles show slightly sharper ADRSs, producing higher gradients. It can be concluded that the anisotropy condition influences the profile but does not significantly change it. This result confirms the applicability of layered specimens for the investigation of deep-lying defects. WRA and QSA are on nearly the same level, up to moderate values of R_m. However, the error in WRA increases significantly when R_m reaches values of

roughly 10, which corresponds to velocities of roughly 6 m/s or 10 m/s for specimens made of copper or aluminum, respectively.

One major drawback of WRA is the absence of the unperturbed lift force $F_z^{(0)}$, which is an immediate result of the decoupling of electric and magnetic fields. The imposed symmetry in $\mathbf{B}^{(p)}$, and therefore also in $\mathbf{J}$, eliminates the lift force after the volume integration. Apart from testing the applicability of different numerical approaches for LET problems, the numerical studies also provide deeper insights into the underlying physics of motion-induced eddy currents.

Measurement and Sensor System

Force Measurement

There is a wide range of techniques available to measure forces. The most common measurement principles of force transducers are introduced with special focus on strain gauge load cells and piezoelectric crystal force transducers. Furthermore, the characteristics of force measurement systems and the importance of calibration have to be considered.

The force is a physical vector quantity that acts on a single point. In order to measure this vector, it has to be translated into a scalar quantity. Since real materials have limited permissible stress, a force cannot be transferred via a single point but always by a finite surface. So strictly speaking, not the force itself is measured but the stress tensor field caused by the force.

A real force measurement system is therefore composed of a force transducer and the associated instrumentation, as well as perhaps mechanical installation aids. A force transducer is a device which converts the applied force into a measurable scalar quantity, e.g., change of electric resistance, through a known physical relationship. The instrumentation associated with a force transducer is used to generate an analogue or digital electrical output to represent the indicated value. Depending on the requirements of the measurement application, the instrumentation may contain a number of separate elements for signal conditioning, indication, analogue-to-digital conversation, and data collection.

Force measurement systems are based on different physical principles but can be described by several common characteristics. The behavior of all these systems can be expressed by plotting the response curve, which represents the indicated output value against the applied force. An ideal response curve is a straight line from zero to the rated capacity of the force measurement system and then back again to zero. Real measurement systems differ from this ideal curve in multiple ways. These are commonly categorized by their systematic deviation with respect to the least squares optimal line through the origin for increasing outputs.

An important concept in measurement systems is known as repeatability which is described by the agreement of the outputs for repeated applications of the same load. In practice, the repeatability of transducers is also provided by many manufacturers.

However, this value can only be a reference for optimal conditions during the testing procedure. In operation it is generally an overestimation of the performance of the force measurement system due to limitations of the actual electrical measurement equipment, present temperature gradients from first to last application, and other environmental influence quantities.

Further characteristics of force measurement systems can be summarized by the imperfections of applying the force to be measured to the loading surface of the transducer. One of the most important specifications is thereby the sensitivity to off-axis forces which result in parasitic torque. For single-component transducers, it is also important to consider the sensitivity to orthogonal forces which is equivalent to misalignment of the transducers' principal axis to the force to be measured.

Differential Lorentz Force Eddy Current Testing Sensor

Based on the LET analysis presented previously, it might be necessary to perform the testing with high velocity, thus using permanent magnet configurations that are better adapted to the current measurement task. Apart from increasing the force perturbations, this would increase the absolute values of the Lorentz force, due to Faraday's law of induction. This could even be a few orders of magnitude larger than the perturbations caused by defects.

Unfortunately, precise measurements of small force variations in a relatively large range of applied forces are very difficult. Thus, there is a strong demand for the usage of differential force measurements in the LET system. Similar tendency is observed in traditional ECT systems as well. In ECT, various differential pickup probe configurations offering higher testing sensitivity have already been designed and successfully implemented (Chari et al. 1990; Mook et al. 2011). Currently, there are several possibilities to obtain the differential force signals resulting from LET system. However, the application of commercially available differential force sensors would lead to higher spatial integration requirements and considerably higher costs. This would be even more important when designing sensor arrays for LET, which could simplify and advance the defect detection and reconstruction, respectively.

Further, a simple and low-cost modification of LET setup is presented which could be used for measurements of differential Lorentz force signals caused by material defects. The proposed modification affects the magnet used where three independent and passive pickup coils have been wound on its surface (Fig. 10). The principal idea is to use voltages induced in the additional coils and correlate the voltage signals with the corresponding differential Lorentz force signals exerted on the magnet. In fact, the resulting magnet system can be applied directly to the existing LET experimental setup, i.e., it can be used as a complete differential Lorentz force sensor. Since this specific modification of the LET system allows differential Lorentz force measurements, the proposed technique has been termed as differential Lorentz force eddy current testing (DiLET).

The concept of the corresponding sensor is based on (Uhlig 2014; Zec 2013; Zec et al. 2015), where a set of passive coils fixed to a PM is proposed to allow the

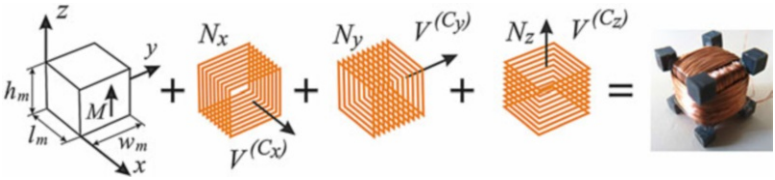

Fig. 10 DiLET – scheme of 3-D differential Lorentz force sensor

detection of perturbations in the eddy current distribution caused by defects inside the specimen.

The main idea of using a simple coil system to obtain the differential Lorentz force signals can be traced back to the following force relation (Haus and Melcher 1989; Ramos and Lopes Ribeiro 2014).

$$\mathbf{F} = \int_{\Omega_M} (\mathbf{M} \cdot \nabla)\mathbf{B} \mathrm{d}\Omega = -\int_{\Omega_C} \mathbf{j} \times \mathbf{B} \mathrm{d}\Omega \tag{12}$$

The primary magnetic field $\mathbf{B}^{(p)}$ produced by a permanent magnet is constant in time, while the secondary magnetic field $\mathbf{B}^{(s)}$, connected with the eddy current distribution inside the specimen, is time dependent when a defect is present. Thus, the induced voltage V_i, $i \in \{x, y, z\}$ in a coil fixed to the PM is proportional to perturbations of the secondary magnetic field $B_i^{(s)}$ and therefore sensitive to disturbances caused by the defect. As shown in (Zec 2013), the induced voltage V_i is proportional to the time derivative of the force component parallel to the respective coil axis.

Optimization of the Permanent Magnet System

Comparative studies between LET and ECT indicated the potential and competitiveness of LET (Carlstedt et al. 2013, 2014). However, the performance of an LET system can be enhanced further by applying optimization schemes to determine advanced magnet systems with improved characteristics.

The optimization goal is to maximize the response resulting from an inclusion surrounded by conductive material, thereby increasing the signal-to-noise ratio and, hence, improving the detection rate. However, due to the large variety of NDT problems, it is self-evident that the final details of an optimized setup strongly depend on the detection goal and external testing conditions for the particular application.

The optimal magnet design is taking into account the tasks to evaluate non-magnetic, electrically conducting specimens. However, it is also applicable to ferromagnetic specimen if the objective function evaluation is adapted to the corresponding requirements. The optimization is performed under the assumptions of a smooth specimen surface and that the defect is located far from any lateral

boundary to neglect parasitic edge effects. Since the resulting Lorentz force profile depends on the shape and the depth of the inclusion, an equivalent defect of cuboidal shape is defined to represent a general flaw. The assumptions can be modified to any particular case of interest, since this would involve only the geometry of the specimens defined in the forward solution, which are described in one of the following sections. The optimization is performed with respect to the drag force F_x and the associated absolute defect response amplitude (ADRA)$\Delta\hat{F}_x$, resulting from the difference between the unperturbed drag force $F_x^{(0)}$ and the perturbed drag force $F_x^{(d)}$. The force profile is symmetric if the interaction between the primary magnetic field $\mathbf{B}^{(p)}$, generated by the permanent magnet, and the secondary magnetic field $\mathbf{B}^{(s)}$, from the induced eddy currents, is negligible.

Figure 11 shows the geometrical parameters of the problem together with the ADRA. The specimen is modeled as a pseudo-infinite half-space including a defect with edge length a, located at a depth d. The magnet system is located at a lift-off distance h above the specimen. The optimization scheme covers but is not limited to isotropic specimens ($\sigma_{xx} = \sigma_{yy} = \sigma_{zz}$) and laminated structures ($\sigma_{xx} = \sigma_{yy} \neq 0$, $\sigma_{zz} = 0$).

Two distinct magnet systems of both scenarios are compared, considering the same magnet volume V_m. For medium-sized deep defects, a cylindrical magnet with a volume ratio of $V_m/V_d = 56$ is chosen to be optimal. The Halbach structure magnet system optimized for small subsurface defects has a volume ratio of $V_m/V_d = 875$. The geometrical parameters are obtained by de-normalizing both systems assuming a lift-off distance and hence geometric scale of $h = 1$ mm. The spatial distribution of the magnitude of the magnetic flux density $\mathbf{B}$ and the induced eddy current density $\mathbf{J}$ is shown in Fig. 12.

The eddy currents for regular cylindrical magnets (Fig. 12a) are less concentrated compared to Halbach systems (Fig. 12b). The Halbach structure leads to a

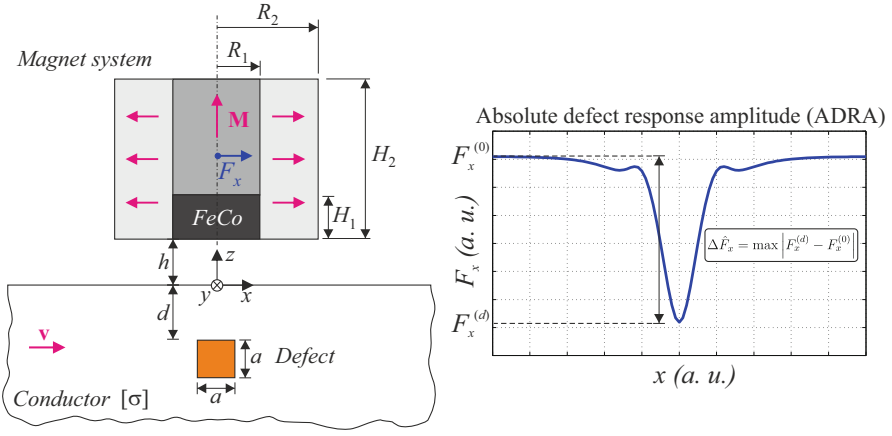

Fig. 11 Parameters of the LET setup, design variables of the magnet system, and depth and resolution, which can be controlled by means of the diameter of the exciting coil (Mook et al. 2007)

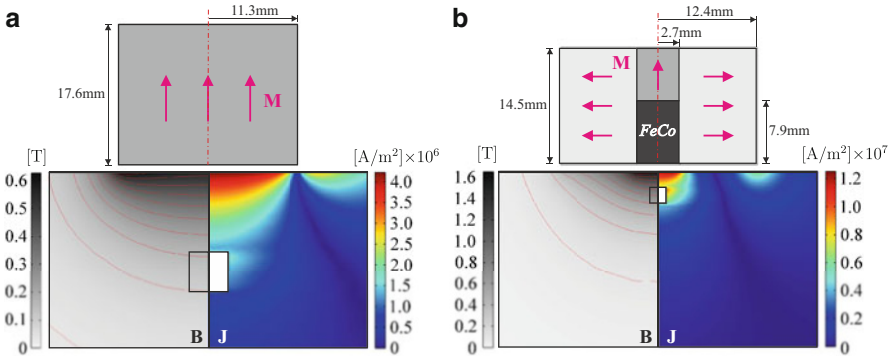

Fig. 12 Magnitude of the magnetic flux density **B** and induced eddy current density **J** of the optimized magnet systems for the case of anisotropic specimens, assuming a lift-off distance of $h = 1$ mm. Both generate an unperturbed drag force of $F_x^{(\mathrm{lab})} = 3$N. Cross section of (**a**) a cylindrical magnet and (**b**) Halbach structure

considerably more focused magnetic flux and eddy current distribution under the inner part of the magnet system. The flux density is increased to 1.6 T on the surface of the specimen, which is significantly larger compared to standard magnet systems (Weise et al. 2015a).

When considering high-speed applications, secondary magnetic fields become prevalent and cannot be neglected. In this case, the magnetic field formulation used in the forward solver can be adjusted (e.g., to an $\mathbf{A}$, $\varphi - \psi$ formulation), albeit at the expense of computational cost. In ECT, there exists a trade-off between penetration the absolute defect response amplitude used as objective function (Weise et al. 2015a)

This fact can be also observed in LET and is inherently a limiting factor of both methods. The results demonstrate the advantage of combining active and passive magnetic materials in the form of a Halbach structure in an LET sensor for selected applications. The results of the unconstrained optimization demonstrate that the use of those structures is counteracting the trade-off between penetration depth and resolution, revealing additional potential of future sensor systems. In the present case, the optimization procedure has been performed considering two different defect scenarios. The associated optimal magnet designs are manufactured and made available for experimental studies presented in (Carlstedt 2016; Mengelkamp 2016). A defect depth study, adopting the concept of a quasi-infinite crack, revealed a current detection depth limit of about 35 mm.

Lorentz Force Evaluation

Nondestructive material testing and evaluation is a vast interdisciplinary field as well as a challenge due to the variety of applications. Whereas the focus of nondestructive testing (NDT) is to detect and localize anomalies within a

specimen, the reconstruction of defect properties (dimensions, shape, structure, composition) and their influence on the material's usability is the focus of nondestructive evaluation (NDE).

Defect identification and assessment are very important aspects of quality assurance. Nondestructive material testing is understood as the noninvasive examination of any type of specimen without changing or altering the properties of the body under test to check whether the specimen contains anomalies. Anomalies are any type of defect or change in the material properties that can be of natural or artificial origin, influencing the usefulness or serviceability of that object (Hellier 2013). Nondestructive testing has turned from a rather empirical procedure dependent on the experience of the examiners into a more quantitative measurement technique that serves to determine the influence of material anomalies on the structural health of the object (Achenbach 2000).

Biomedical applications often require the determination of electrical conductivity of human tissues. It is a common approach to use induction coils inducing electrical currents in the tissues. This results in changes of the coil's impedances. These changes are used to obtain information about the tissue conductivity. Similarities and dissimilarities between appropriate sensor setups have been investigated and compared for biomedical applications (Petković 2013). A very similar approach can be used to determine the conductivity distribution of metallic specimen. If the permanent magnet system is approximated by a dipole model, the same strategy for the solution of the inverse problem can be applied. This serves as the basic idea for proposing a new method for noncontact, nondestructive evaluation of solid conductive materials, termed Lorentz force evaluation (LFE). In contrast to the bioelectromagnetic application, where magnetic flux is measured at points above the conductor, in LFE the Lorentz force acting on a permanent magnet moving relative to the specimen is measured.

The inverse problem of the LFE technique, which has been introduced for inverse calculations of LET signals in (Petković et al. 2013), is to characterize the geometry of the underlying defects. A straightforward approach is applied to solve this inverse problem directly and estimate the defect parameters. The geometrical parameters of the defect, such as the center of gravity, depth, and extension, can be defined as the unknown variables. Other approaches are to determine the eddy current distribution and the conductivity distribution in the conductor. In these reconstruction approaches, the solution vector can compose the unknown moments of the equivalent current dipoles or the unknown voxel conductivities. Solving an inverse problem implies the minimization of the error between measured data and forward calculated data with respect to the unknown parameters.

Material anomalies, such as changes in conductivity, defects, cracks, or inclusions, distort the eddy current distribution in the object under test and, consequently, also the Lorentz force measured at the magnetic system. Thus, defects/anomalies in the conductive material produce perturbations in the Lorentz force signals. Extensive basic research has been done to show that the direct relationship between changes in force and material anomalies can be used to detect defects. If the detected defect has to be identified with respect to depth, material properties,

and shape reconstruction, the procedure is called motion-induced eddy current testing and evaluation (MIECTE).

In general, the defect response signal (DRS) defined as the difference between the Lorentz force determined for the defective object and the defect free object is used in MIECTE. In the simplest approach (Petković et al. 2013), the DRS can be estimated using a set of current dipoles located only in the defect region (Fig. 13). The current dipoles are calculated from the distribution of eddy currents determined for the defect-free conductor. However, the DRS found in this way is far from the actual signal because it does not take into account the disturbance of the flow of eddy currents around the defect. DRS quality can be improved by the use of the so-called extended area approach (EAA) in which the influence of disturbed eddy currents flowing around the defect is taken into account (Ziółkowski 2015).

In the LFE, minimum norm estimation methods are often applied to the reconstruction of eddy current distributions, which are responsible for defect response signals that are measured by the LET system (Fig. 14). Solving an inverse problem in a fully three-dimensional source space requires the use of high computational resources, including large memory space and long computation times. In order to avoid the inversion of very large kernel matrices, the defect reconstruction procedure can be divided into three steps: (1) determination of a depth of the intermediate plane

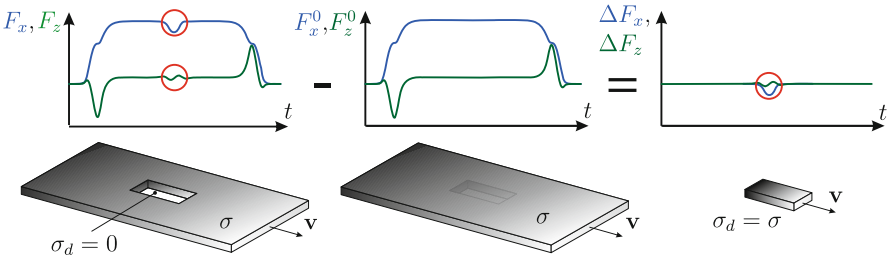

Fig. 13 Simplest approach for modeling a defect response signal from a defect in a conductive specimen

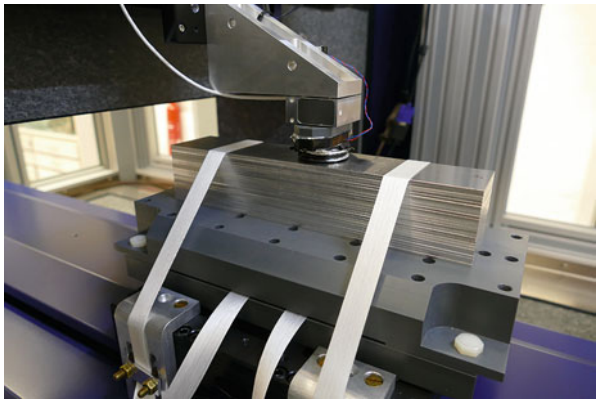

Fig. 14 Experimental setup for the LET measurements in the laboratory

of a defect, (2) determination of the length of a defect in a moving direction of a specimen, and (3) reconstruction in the defect midplane parallel to the upper surface of the bar and the scanning plane. Determination of the depth of long defects can be precisely determined using both measurement and data obtained by finite element method (Petković et al. 2013). In the case of wide defects, a depth of its intermediate plane is slightly moved toward the surface but still being in an acceptable range of error (i.e., less than 1 mm). Determination of a subsurface defect depth involves as much as possible a priori knowledge about the defect, e.g., it is usually assumed that in the specimen exists only one defect and the type of the defect is known. The length of such a defect with main orientation in the direction of movement of the solid bar was successfully determined in all cases, whereas the reconstruction in the plane parallel to the conductor upper surface was satisfactory as well. The results have indicated that LET and LFE have a great potential for investigating defects in non-ferromagnetic conductors, especially in laminated composites.

The Lorentz force evaluation (LFE) can be regarded as an interesting alternative to the well-established eddy current testing technique, when in a non-ferromagnetic moving conductor deep internal defects/anomalies have to be identified. In such cases, complicated structures with moving components lead to very high computational costs, i.e., is highly preferable to apply fast numerical models to solve the forward problem. Solving the inverse problem, i.e., the identification of defects or conductivity anomalies, requires efficient solution strategies. In most cases, the number of optimization methods that can be applied for this purpose is limited because usually only derivative-free methods can be used. There is a need of much more research, in particular in the use of stochastic optimization methods for the development of efficient solution strategies. Nevertheless, the application of different inversion algorithms (including improved forward modeling in the defect region) and regularization techniques or usage of more complex permanent magnet configurations (to generate a maximum magnetic flux density) defines the next steps to improve the reconstruction accuracy of the LET and LFE as options of the motion-induced eddy current testing and evaluation.

Applications

In industry, the market share of composites is increasing fast, and composites are now widely used in the aerospace industry, the automotive industry, the marine industry, etc. They can be found in ship hulls, floor panels, architectural claddings, etc. The composites industry continues to evolve. There is a huge potential for a similar technology shift in the architectural and building and construction segments as the industry takes advantage of the design flexibility, durability, low weight, corrosion resistance, and other properties that composites offer. Composite materials have fueled the growth of new applications in markets such as transportation, construction, corrosion resistance, marine, infrastructure, consumer products, electrics, aerospace, appliances, and business equipment. They are used in industrial applications where corrosion resistance and performance are critical. Fiberglass is often used as the reinforcing fiber. Industrial composite products include underground

storage tanks, scrubbers, piping, fume hoods, water treatment components, and pressurevessels. The aerospace industry, including military and commercial aircraft, is the major customer for advanced composites

Due to the complex structures of the composites with very different and often not precisely known material properties, it is difficult to provide appropriate techniques for testing and evaluation. If the MIECT technique should be applied, only electrically conducting materials can be evaluated, i.e., with NDT methods like LET, the conductive components of the composite devices can be evaluated because there the eddy current flow is induced. Furthermore, the evaluation of composite materials and in particular the identification of defects or conductivity anomalies need the numerical modeling of the eddy current flow in these conducting components. Thus, in the following section, laminated composite materials will be considered.

Inspection of Glass Laminate Aluminum Reinforced Epoxy

Composite materials can withstand stronger mechanical stress, but at the same time, they are a big challenge for nondestructive testing and evaluation. In this section, measurement results using LET for Glass Laminate Aluminum Reinforced Epoxy (GLARE) samples are presented and compared with simulations (Brauer et al. 2017; Gorges et al. 2016). GLARE is a fiber metal laminate (FML) composed of several very thin layers of metal (usually aluminum) interspersed with layers of glass-fiber bonded together with a matrix such as epoxy. The unidirectional prepreg layers may be aligned in different directions to suit the predicted stress conditions. Figure 15a shows a composition of eight aluminum (light gray) and seven glass-fiber laminate layers (dark gray). In the study presented here, two GLARE samples (aluminum alloy No 3.1354, $\sigma_0 = 17$MS/m) shown in Fig. 15b are used. Both specimens are 350 mm × 150 mm and made of 5 aluminum sheets, each 0.4 mm thick, with

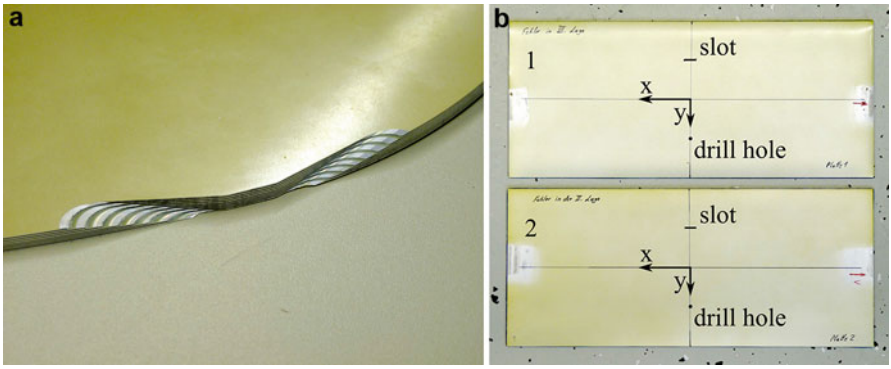

Fig. 15 Test specimen (GLARE): (**a**) test piece of A380 fuselage (cabin window); (**b**) two specimens (each 350 mm × 150 mm) with machined defects included in the second aluminum layer (2) and third aluminum layer (1); the same defects in both *Al* layers: a drill hole (diameter = 2 mm) and a through slot (1 mm × 10 mm)

0.25 mm glass-fiber laminate between the sheets, resulting in a total thickness of the specimen of 3 mm. Both specimens have as machined defects a slot (10 mm × 1 mm) and a drilled hole (diameter = 2 mm) at the marked spots in one of their aluminum layers. Specimen 1 has the defects in the third aluminum layer (defect depth = 1.3 mm) and specimen 2 in the second layer (defect depth = 0.65 mm), counted from the top layer.

The experiments have been performed on the multipurpose measuring platform BASALT-C MMP-15 available at our university laboratory (Fig. 16) (TETRA Gesellschaft 2015). In the study two magnet systems have been used, either a cylindrical permanent magnet or the Halbach system positioned above the GLARE specimen at a lift-off h (Fig. 17) (Gorges et al. 2016). The sample specimen is mounted onto the x-slide. The slide moves the specimen with a constant velocity crossing the magnetic field B_0 produced by the magnet system. Due to the relative motion between B_0 and conductive parts, eddy currents are induced in the specimen resulting in the Lorentz force acting on the specimen. The corresponding counterforce $\mathbf{F} = [F_x, F_y, F_z]^T$ is exerted on the magnet and is measured with a three-axial strain gauge force sensor. The force sensor used during measurements is

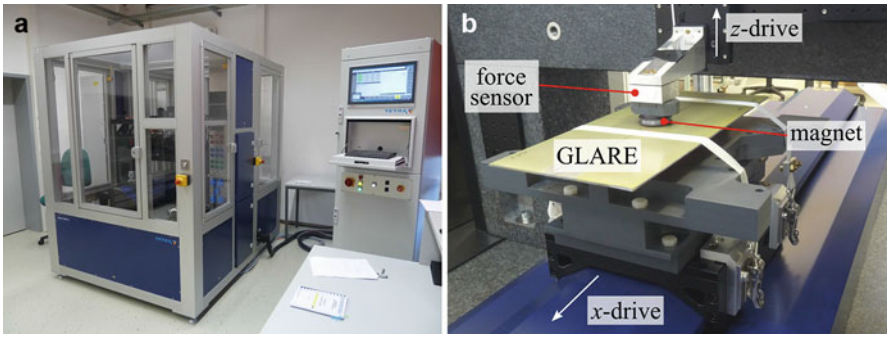

Fig. 16 Measurement setup for GLARE specimen: (**a**) multipurpose measurement platform MMP-15 and (**b**) LET measurement of GLARE specimen

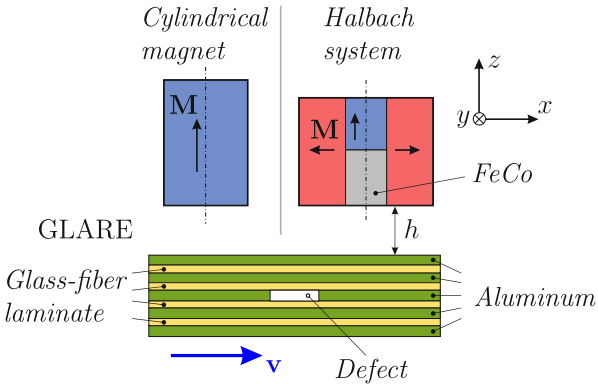

Fig. 17 LET experiment setup for GLARE samples and different magnet systems

the K3D40, a triaxial sensor with ±2 N nominal force in all three directions (ME-Meßsysteme 2014). The LET experiments were carried out at the specimen velocity of $v = 200$ mm/s and the lift-off distance $h = 1$ mm. The y-coordinate was incremented by 0.5 mm over the 150 mm width of the specimen. The cylindrical magnet and the Halbach structure were used to obtain scans of force profiles for various GLARE specimens (Fig. 18). The surface scan leads to a plot of the lift force profile shown in Fig. 18 obtained for the GLARE sample presented in Fig. 15b.

Figure 19 shows the measured drag and lift forces along the centerline of the specimen, where no defect is present. The leading edges of the specimen entered the magnet field at $x \approx -175$ mm. The trailing edge left the magnet field at $x \approx -175$ mm. The lift force F_z has a positive and negative peak at these positions,

whereas the drag force F_x rises to a plateau and drops back to zero. Figure 19a shows that the plateau has a dent, which is caused by the uneven surface resulting in a change of the lift-off distance. Both the cylinder magnet and the Halbach system

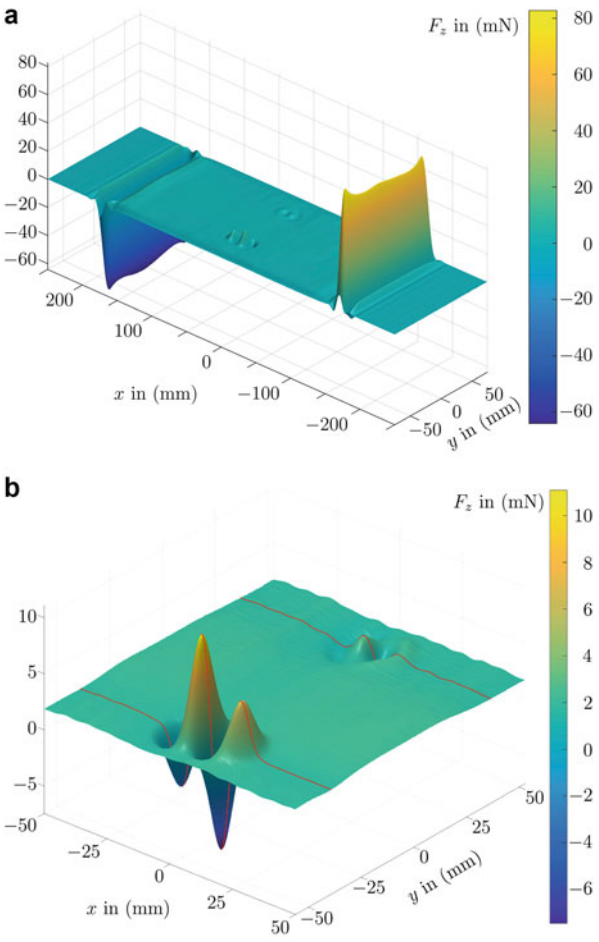

Fig. 18 Sample LET scan of lift force profile (F_z) for the GLARE specimen with two defects: (**a**) total scan and (**b**) zoom into the region around the defects

show this behavior. Using the Halbach configuration, the maximum forces are clearly higher, and the general force profile is sharper comparing to the cylindrical magnet. This is the result of the focused magnetic flux density produced by the Halbach system. Because the design of this sensor leads to a field-focusing effect just below the magnet bottom, much higher magnetic flux density values can be achieved. This results in significantly higher Lorentz forces (especially for the drag force) which are about 25%–30% higher than those for the cylindrical permanent magnet.

Figure 20 shows a comparison of the Lorentz force acting on the magnet depending on the defect depths. Here only the results for the Halbach system are shown.

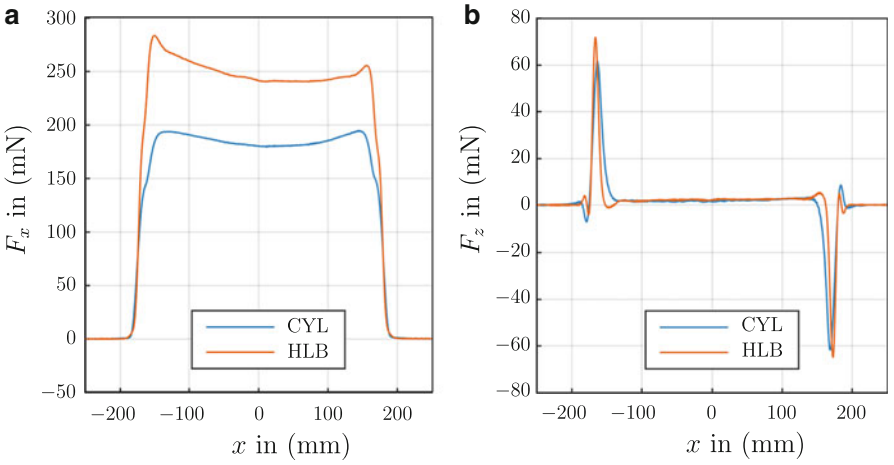

Fig. 19 Measured forces exerted on the cylindrical magnet (CYL) and Halbach system (HLB)

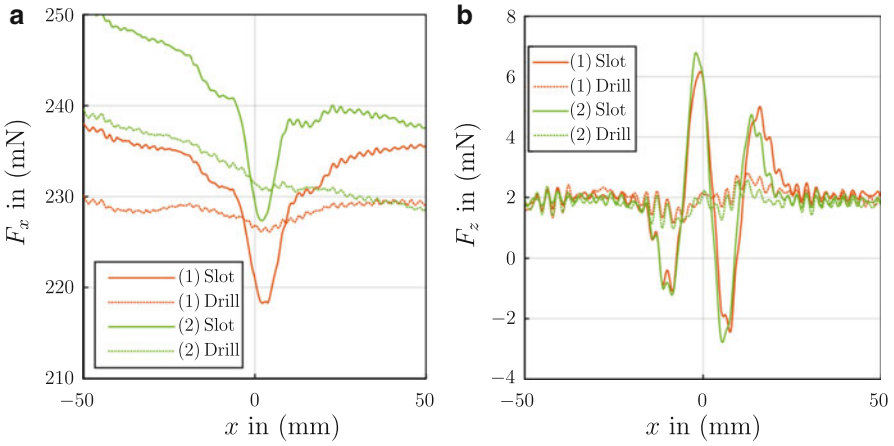

Fig. 20 Measurements of the Lorentz force exerted on the Halbach structure by scanning both GLARE samples (see Fig. 15b) which is moving in the x-direction

The plots are cropped to the range $-50\ \text{mm} \leq x \leq 50\ \text{mm}$. The solid lines correspond to the slot defect while the dotted lines to the drill hole defect. The results for GLARE specimen (1) and (2) are depicted with red and green color, respectively.

It can be noted that the deformed uneven surface affects F_x a lot and makes it difficult to find out, where the deeper defect is located (Fig. 20a). In Fig. 20b, it can be observed that for specimen (2), the deflections caused by the slot defect are a little bit larger than for specimen (1). Since specimen (2) has the defects in the second aluminum layer, they are 0.65 mm closer to the magnet system than in specimen (1), and this indeed results in a stronger deflection in the force. The drill hole is hardly distinguishable in the z-component. From the drill hole signals, it cannot be concluded which is the deeper defect, since the noise oscillations in the signal are too high (Brauer et al. 2017; Gorges et al. 2016).

It has been shown that the cylindrical Halbach structure has, compared to a cylindrical permanent magnet, a superior performance in detecting small subsurface defects (Weise et al. 2015a). The normalized root-mean-square error (NRMSE) between the numerically calculated and measured Lorentz force signals is used to define the goal function. A finite element model is used to calculate the magnetic flux density, including the extended area approach for the force calculation.

The goal function scanning (GFS) method has been applied to solve the inverse problem described in Fig. 15b, i.e., to identify the two defects at different depths (Mengelkamp 2016; Mengelkamp et al. 2016; Storn and Price 1997). Therefore, the landscape of the goal function is investigated for a set of grid points uniformly distributed in the search space. Since the GFS method is limited to one defect, it is evident to use the geometry parameters of the defect as design variables. Then, the location of the defect, i.e., the x- and y-coordinates of its center of gravity, can be determined easily. The defect location is assigned to the position at which the ΔF_x-component of the DRS has the largest absolute amplitude.

The GFS is applied to each aluminum layer separately. The results show that there exists one local minimum in each single aluminum layer. Thus, if the optimization function is considered separately for each layer, it is convex. The minimum NRMSE in the five layers corresponds to the correct defective second layer. It has been observed that with the increasing depth of the metal layer, the defect extensions corresponding to the local minima in the single-layer increase. Furthermore, because the goal function is relatively flat, the minimums cannot be distinguished precisely (Mengelkamp 2016). Much more research is required to adapt appropriate solution strategies to this kind of inverse problems.

Defectoscopy of Friction Stir Welding

Friction Stir Welding

Friction stir welding (FSW) is a solid-state joining process that uses a non-consumable tool to join two facing workpieces without melting the workpiece

material. It was invented and experimentally proven at The Welding Institute (TWI), Cambridge/UK, in 1991 (Dawes and Thomas 1996; Thomas et al. 1991). A non-consumable rotating tool with a specially designed pin and shoulder is inserted into the abutting edges of sheets or plates to be joined and traversed along the line of joint (Fig. 21). The tool serves two primary functions: (a) heating of the workpiece and (b) moving the material to produce the joint. The heating is accomplished by friction between the tool and the workpiece and plastic deformation of the workpiece. The localized heating softens the material around the pin, and the combination of tool rotation and translation leads to movement of material from the front of the pin to the back of the pin. As a result of this process, a joint is produced in solid state. During the FSW process, the material undergoes intense plastic deformation at elevated temperatures, resulting in generation of fine and regular recrystallized grains. The fine microstructure in friction stir welds produces good mechanical properties (Mishra and Ma 2005; Mishra et al. 2014).

FSW is emerging as a very effective solid-state joining technique. In a relatively short duration after its invention, several successful applications of FSW have been demonstrated. FSW is primarily used on wrought or extruded aluminum and for structures which need very high weld strength. Therefore, FSW is particularly found in modern shipbuilding, trains, and aerospace applications. In addition to aluminum alloys, friction stir welding has been used successfully to join other metallic materials, such as copper, titanium, steel, magnesium, and composites. Because of high melting point and/or low ductility, successful joining of high melting temperature materials by means of FSW was usually limited to a narrow range of FSW parameters. Preheating is beneficial for improving the weld quality as well as increase in the traverse rate for high melting materials such as steel (Reddy and Reddy 2016). Despite considerable interests in the FSW technology in the past decade, the basic physical understanding of the process is adverse. Some important aspects, including material flow, tool geometry design, wear of welding tool, microstructural stability, and welding of dissimilar alloys and metals, still require deeper understanding. However, it can be observed that new technologies are often commercialized before a fundamental science emphasizing the underlying physics can be developed. This seems to be the case for the FSW technology as well.

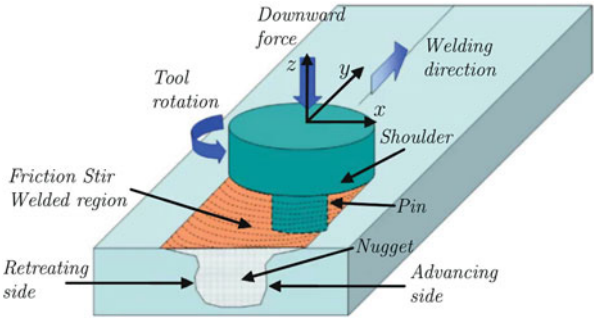

Fig. 21 Schematic drawing of the principle of friction stir welding (Mishra and Ma 2005)

Imperfections/Defects Caused by Friction Stir Welding

In the different zones of the stirred region, the physical behavior of the material as well as the selected welding parameters during the welding process will cause different potential defects (Fig. 22). The tool geometry is a very important factor in producing sound welds. However, at the present stage, tool designs are generally proprietary to individual researchers, and only limited information is available in the open literature. From the literature it is known that a cylindrical threaded pin and concave shoulder are widely used welding tool features. The welding parameters, including tool rotation rate, traverse speed, spindle tilt angle, and target depth, are crucial to produce sound and defect-free welds. Thus, the design of the tool shoulder together with the applied force pushing the tool on the specimen surface, the rotational speed of the tool, and the speed of welding along the specimen has an important impact on the degree of changes of the material plasticity and on the potential appearance of defects. Thus, FSW can be associated with a number of imperfections or defects if it is not performed properly (Fig. 22).

Insufficient weld temperature, due to low rotational speed or high traverse speed, for example, means that the weld material is unable to accommodate the extensive deformation during welding. This may result in long, tunnel-like defects (so-called wormholes) running along the weld, which usually occur inside the welding seam (Fig. 23). The wormholes appear if process parameters are not correctly chosen and the heat input is insufficient. This happens if either the force the tool is pushing on

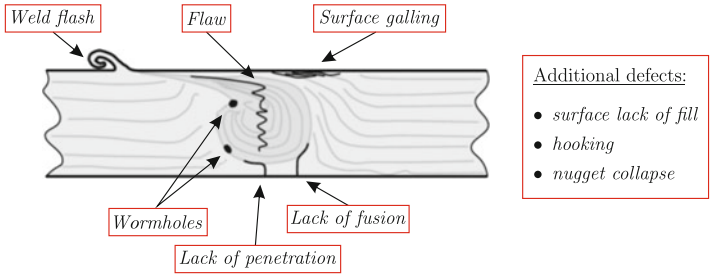

Fig. 22 Typical defects/imperfections which can be found in or around the welding zone (Voellner 2010)

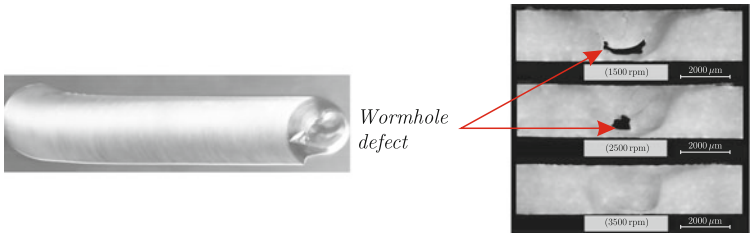

Fig. 23 Wormholes appearing in the welding zone if the force on the tool or its rotational speed is too low (Voellner 2010)

the material is too low or the rotational speed of the tool is too low. The appearance of wormhole defects can be reduced by increasing the rotational speed. On the other hand, if the generation of wormhole channels is a desired effect, this can be achieved by means of tuning the welding speed. In this way, e.g., cooling channels might be realized inside the welding seam.

Nondestructive Testing of Friction Stir Welds

Numerous imperfections or defects have been defined in the literature (Kim et al. 2006; Pietras and Weglowski 2014; Voellner 2010). Unfortunately, these defects cannot be identified in a nondestructive way so far. The following Al-specimens have been welded using the robot-based setup of the Production Engineering Lab at the Technische Universität Ilmenau. This FSW station uses a KUKA six-axis joint-arm robot. Two pieces of Al alloy (thickness = 8 mm) were joint on this FSW system (Fig. 24). The following process parameters have been chosen:

- Material: *Al*-alloy, EN AW 6060 T66
- Dimension: 300 mm × 100 mm × 8 mm
- Feed rate: 400 mm/min
- Tool rotation speed: 2000–3000 rpm
- Tool force: 8 kN
- Surface treatment: milled

The main goal of this study was to analyze whether the MIECT technique is able to evaluate the welding zone properly. It should prove which imperfections/defects can be found in or close to the welding seam, because FSW is well known for its reproducibility and freedom from traditional fusion welding imperfections such as shrinkage cavities or slag inclusions.

If FSW should be widely accepted as a joining method, reliable, but also cost-effective process, specific quality assurance activities have to be developed. So far there is neither a common standard defect catalogue for FSW, which summarizes all relevant irregularities and describes their allowable sizes for different applications,

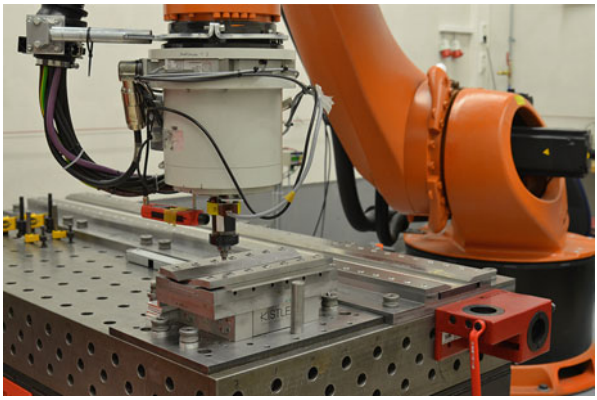

Fig. 24 Robot-based FSW of aluminum specimen in the Production Engineering Lab at the Technische Universität Ilmenau, Germany

nor a standardized test specification for FSW welds. Moreover, it is not even fully understood how different imperfections of the weld are affecting its mechanical properties during static and dynamic loads.

Off-line methods include nondestructive tests, commonly applied in welding engineering and in testing the quality of FSW joints. Most popular NDT methods include visual testing, penetrant inspection, ultrasonic examination, X-ray testing, and eddy current testing. Other useful techniques include modern methods such as synchrotron radiation and computer tomography (Pietras and Weglowski 2014). Standards (EN ISO 25239-5 and AWS D17.3) recommend the following NDT methods for testing FSW welding imperfections (American Welding Society 2016; German Institute for Standardization 2015):

- Visual testing (VT)
- Liquid penetrant inspection (LPI)
- X-ray testing (CT)
- Ultrasonic testing (UT)

In addition, the standard AWS D17.3 enables application of other tests such as acoustic emission, eddy current testing, neuron radiography, leak tests, etc. Individual types of tests have various intended uses and various levels of detectability of specific welding imperfections. Eddy current testing of FSW joints is used, but it is not one of the techniques that are explicitly recommended by the standard for the inspection of FSW joints (German Institute for Standardization 2015). In the case of thin joints, imperfections could be expected in the whole cross section. Eddy current testing of FSW joints requires individually designed transducers, which optimizes the technique (dos Santos et al. 2008; Pitkänen et al. 2014; Rosado et al. 2010). The detection of conventional flaws, like the lack of penetration and lack of fusion, is an important and challenging NDT task. The usage of conventional EC probes demonstrates there is no distinctive signal feature that can allow the distinction between each defect conditions. In order to improve the reliability of nondestructive inspection using eddy current testing in FSW, alternative methods or new probes have to be introduced.

MIECT Measurements of Friction Stir Welds

The current situation for nondestructive testing of friction stir welds is characterized by the application of only a few conventional techniques (visual inspection, ultrasound, liquid penetrant inspection, computed tomography), as mentioned in the standards (German Institute for Standardization 2015). Electromagnetic testing methods like eddy current testing are not widely spread. But if metals such as aluminum have to be investigated, it is worth to take into account the utilization of the MIECT technique to identify imperfections or defects in the welding region. It is important to know what happens below the surface and deeper inside the welds or in the welding zones. In the previous section, aluminum alloy specimen has been joint by means of the FSW system available in the Production Engineering Lab. This sample has been used for MIECT measurements on the MMP-15 platform, where

the main goal was to identify different depths of the lack of penetration or perhaps other imperfections/defects in or near the welding zone (Fig. 25). The parameters used for the MIECT measurements are:

- Magnet: cylindrical Halbach structure (with DiLET coil)
- Orientation of specimen: welded side facing the magnet
- Velocity: 200 mm⁄s
- Lift-off distance: 1 mm
- Scan width: −30 mm (0.5 mm step) 30 mm
- Sampling frequency: 1000 Hz
- Low-pass cutoff frequency: 50 Hz
- Scanline repetitions: 25

During the movement of the FSW sample in the vicinity (lift-off distance = 1 mm), the profiles of the Lorentz forces exerted on the permanent magnet have been measured. Both the drag force F_x and the lift force F_z were recorded while moving in the x-direction.

Figure 26 shows the measured force along the length of the specimen, i.e., in a small band (60 mm) along the welding zone around the central line ($y = 0$), just above the welding seam. If there is no disturbance due to imperfections or defects, the drag force profile has a plateau over the entire length of the specimen. In this case, it can be clearly seen that the welding changes the conductivity distribution, compared to the region outside the welding zone. The starting point and the end point of welding can be identified as well as an additional defect close to the end point. It can be observed that at the defect position, the force signal is significantly smaller than in the vicinity. This means that there is a remarkable difference in the electrical conductivity in the welding zone due to friction and stirring or due to defects, e.g., a hole in the seam. This has been confirmed by a follow-up visual inspection.

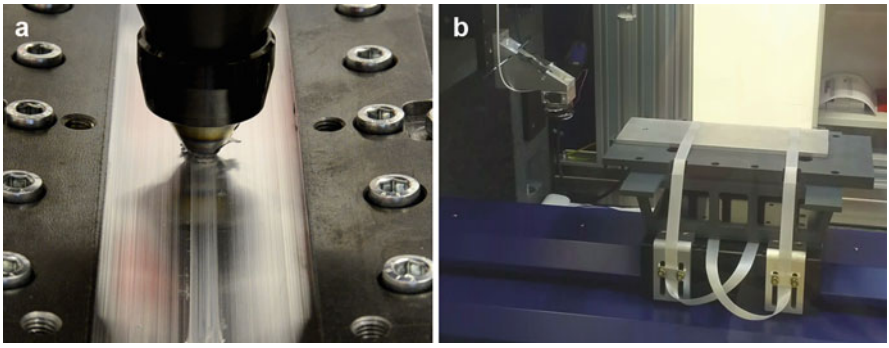

Fig. 25 (**a**) Friction stir welding of the *Al* specimen; (**b**) MIECT measurement of the FSW specimen on MMP-15

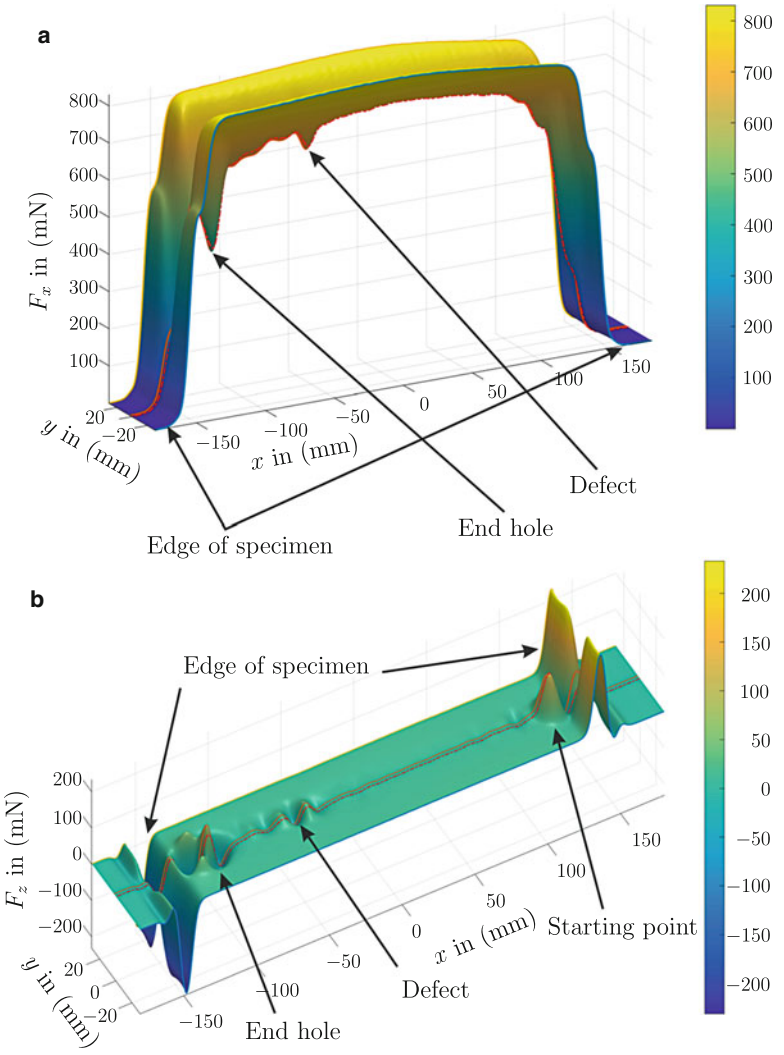

Fig. 26 Force measured along the friction stir weld (red dashed line)

It is obvious that the lift force is more sensitive to the conductivity changes in the welding zone. Again, the edge effect caused by the ends of the sample gives the largest signal. Further, it can be seen that the sample has not been joint to the end of the specimen, because the force signal is zero in those regions. On the other hand, the lift force signals contain obviously more information of the internal defect than the drag force, leading to more details in the force profile around the defect.

The signals shown in Fig. 27 are the result of some post-processing of drag force and lift force. It turned out that the lift-to-drag ratio, i.e., the relation of lift force to drag force, reduces the sensitivity to the lift-off distance and conductivity deviations.

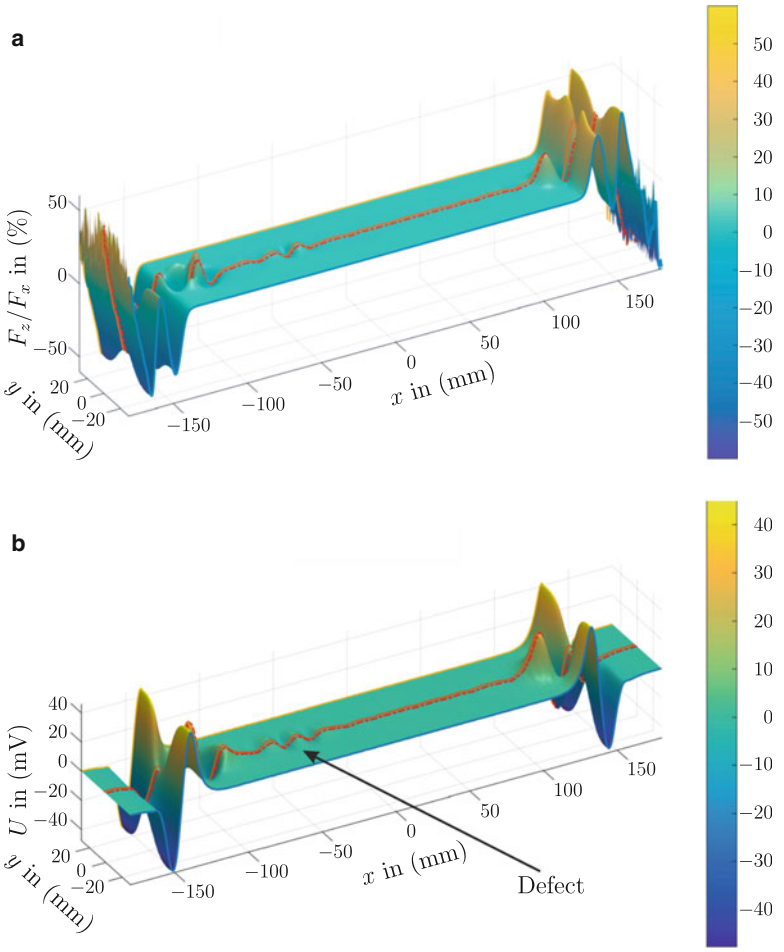

Fig. 27 Lift-to-drag-force ratio and DiLET signal measured along friction stir weld

This results in data which show higher contrasts than the signals separately. The position of the defect can be identified in this figure at about 2.5 mm beside the centerline (red dashed lines). Furthermore, another near-surface defect has been located close to the starting point. This unexpected finding has been identified afterward as a micro-defect, not visible at the surface.

In a second measurement, a DiLET sensor has been used. This is a differential sensor consisting of a permanent magnet configuration combined with a coil containing a large number of windings. In this sensor system, the motion of the specimen in the static magnetic field will induce a voltage in the coil. This voltage is measured and is used for the defect detection. If the magnet system has been optimized with respect to the desired kind of measurement task, a much higher magnetic flux density can be achieved in the region of interest. The magnitude of the

measured voltage is proportional to the velocity, i.e., increasing the measurement speed will lead to higher voltage signals, presupposing the sampling rate is high enough.

The DiLET sensor generally yields to a higher sensitivity of the entire sensor system, but it leads also to rather noisy data, which can be observed as ripples in Fig. 27b. On the other hand, the voltage profile confirms the position of the defect at 2.5 mm beside the centerline, which is probably a lack of fusion (Fig. 22). This result confirms basically the finding with the common force sensor (Fig. 26).

Potential Applications of MIECT

Nondestructive Defect Detection

The general aim of nondestructive testing techniques applied to FSW is the detection of imperfections and/or defects. This includes the determination of the electrical properties (e.g., electrical conductivity) as an alternative for the peak-to-peak measurement, the estimation of the oxide band (so-called kissing bonds), the identification of nugget collapses, or the investigation at both the advancing and the retreating sides of the welding joint. Further, it would be very helpful to provide a technique to identify any lack of penetration from the welding surface in a nondestructive way, especially for thick material components, i.e., much thicker than the penetration depth of the electromagnetic field.

Material Science

There is a high potential for the development of the MIECT technique if the structure transformation in different materials during welding can be evaluated. The investigation of grain size-affected properties in similar and dissimilar aluminum alloys is a promising field of application, with a high impact on lightweight constructions or aircraft engineering. Furthermore, the interaction between process parameters and grain structure is highly interesting. This include the improvement of the understanding of the necessary structural adjustment for components with high static and dynamic stresses, the entire friction stirring process, or the electrical characterization of the interfaces between different grain sizes.

Process Control and Monitoring

An important improvement would be the integration of the MIECT into the welding process itself, either for surface-based inspection or for weld root-based inspection. This would generally qualify the whole process monitoring, both with a tracking system for the process control and with an independent, nondestructive weld seam inspection for the quality control of the welding process.

Ferromagnetic Materials

This chapter focuses on the application of MIECT methods and in particular LET in the framework of non-ferromagnetic materials. However, the moderate rate of change of the magnetic field with respect to the specimen together with the application of NdFeB magnets with high energy densities leads to considerable

advantages in terms of penetration depth, which is the physical limit of traditional ECT. Therefore, the goal is to provide an outlook and to reveal the potential of the MIECT/LET method regarding its usage in combination with ferromagnetic materials. Typical areas of application are, for example, railway testing, steel casting, or pipeline inspection, where safe operation is paramount. In most application scenarios, motion is inherently present and already part of the operation, which privileges MIECT in general especially when it comes to online and in process inspection. Because of distinct differences in the underlying physics, it cannot make claims to completeness since it would require a comprehensive retreatment of the content presented this far. The principled approach of MIECT in case of ferromagnetic specimen resembles the principle of magnetic flux leakage (MFL) (Shi et al. 2015), which is one of the most popular methods of pipeline inspection. In MFL, the specimen is subject to an external magnetic field. Defects are detected on the basis of the leakage of the magnetic field, i.e., $\mathbf{B}^{(p,s)}$, which is sensed by, for example, Hall effect sensors or GMRs (Shi et al. 2015). However, MIECT extends the principle to moving parts.

The nonlinear relationship between the magnetic field and the magnetic flux requires a reformulation of the governing equations. The primary magnetic field $\mathbf{B}^{(p)}$ is now altered in the presence of the ferromagnetic specimen. Therefore, it can be further divided into a part containing only the magnetic flux generated from the permanent magnet itself as in the case of non-ferromagnetic specimen $\mathbf{B}^{(p,m)}$ and into a distorted part, resulting from the ferromagnetic specimen $\mathbf{B}^{(p,s)}$ such that $\mathbf{B}^{(p)} = \mathbf{B}^{(p,m)} + \mathbf{B}^{(p,s)}$. The backreaction of the motional eddy currents, i.e., their magnetic flux, is the secondary part $\mathrm{B}^{(s)}$. One fundamental difference compared to non-ferromagnetic specimen is that the distorted part of the primary field $\mathbf{B}^{(p,s)}$ leads to considerable Kelvin forces attracting the magnet to the specimen. In this way, the Kelvin force acts against the Lorentz force and a complex interaction between both forces can be observed. Another elementary difference arises when considering the presence of a defect and the time derivatives of the mentioned field components. Now, in additional to a varying secondary magnetic field from the induced eddy currents ($\partial\mathbf{B}^{(s)}/\partial t \neq 0$), the distorted part of the primary magnetic field changes over time as well ($\partial\mathbf{B}^{(p,s)}/\partial t \neq 0$). The latter plays a key role and privileges the application of differential magnetic field sensors, e.g., coils, to sense field variations in addition to the force as it is presented in section "Differential Lorentz Force Eddy Current Testing Sensor."

This requires changes of the numerical simulation environments and additional effort to propose efficient approaches since nonlinear magnetic materials involve higher computational cost because of the usage of iterative solvers. Note that some of the semi-analytical approaches include the possibility to model linear ferromagnetic materials (Reitz 1970; Reitz and Davis 1972; Saslow 1992; Ziółkowski 2015). This is incorporated in the analysis of oscillatory motion as well (Amati et al. 2007; Ooi 1977; Ooi and Jain 1979; Weise 2016; Weise et al. 2015b), which could serve as reference solutions for first numerical simulations and implementations thereof.

The availability of efficient numerical approaches would enable the revision of optimal magnet designs by replacing the proposed forward model and a possible

redefinition of the quantity of interest depending on the applied sensor system. The remaining procedure of the proposed optimization strategy remains unaltered because of its general form. In the same course, the uncertainty and sensitivity analysis should be retreated in order to identify the most influencing parameters. The uncertainty analysis of nonlinear magnetic materials is more intricate, but information about its treatment can be found in (Roemer et al. 2014). Note that because of the attraction and magnification of the magnetic flux into the specimen, the useful signal will be influenced positively by being more sensitive with respect to the material properties of the specimen.

The major differences also necessitate a revision of the experimental setup and the applied sensors. Because strong Kelvin forces are present, the lift-off distance between the magnet and the specimen plays a major role during the design process of new systems. In addition to the Lorentz force, magnetic field sensors such as coils, Hall sensors, or GMRs are of particular interest depending on the final application. Perhaps the greatest influence of introducing ferromagnetic materials can be observed in terms of defect evaluation and in solving the inverse problem. The difficulty, as pointed out in the preceding discussion, lies in the estimation of the primary magnetic field distribution $\mathbf{B}^{(p)} = \mathbf{B}^{(p,m)} + \mathbf{B}^{(p,s)}$ and the associated eddy current distribution. Efficient forward models would again provide an indispensable starting point. A promising solution approach lies in the use of magnetic dipoles in addition to the presently used current dipoles to determine the total magnetic flux and the resulting eddy current distribution.

Notwithstanding the above, the introduction of ferromagnetic materials engenders a series of new challenges. The calculation of the electromagnetic fields is more complex and costly and so are all related tasks depending on those. However, applications such as in-service high-speed railway inspection give reason enough to pursue the effort to further elaborate the MIECT method in this direction.

References

Achenbach JD (2000) Quantitative nondestructive evaluation. Int J Solids Struct 37(1–2):13–27

Amati N, Tonoli A, Canova A, Cavalli F, Padovani M (2007) Dynamic behavior of torsional eddy-current dampers: sensitivity of the design parameters. IEEE Trans Magn 43(7):3266–3277

American Welding Society (2016) Specification of friction stir welding of aluminum alloys for aerospace. AWS D17.3/D17.3M

Antunes OJ, Bastos JPA, Sadowski N, Razek A, Santandrea L, Bouillault F, Rapetti F (2006a) Comparison between non-conforming movement methods. IEEE Trans Magn 42(4):599–602

Antunes OJ, Bastos JPA, Sadowski N, Razek A, Santandrea L, Bouillault F, Rapetti F (2006b) Torque calculation with conforming and non- conforming movement interface. IEEE Trans Magn 42(4):983–986

Biddlecombe CS, Simkin J, Jay AP, Sykulski JK, Lepaul S (1998) Transient Electromagnetic Analysis Coupled to Electric Circuits and Motion. IEEE Trans Magn 34(5):3182–3185

Binns KJ, Lawrenson PJ, Trowbridge CW (1992) The analytical and numerical solution of electric and magnetic fields. Wiley, Chichester

Bird J, Lipo TA (2009) Modeling the 3-D rotational and translational motion of a Halbach rotor above a split-sheet guideway. IEEE Trans Magn 45(9):3233–3242

Brauer H, Ziolkowski M (2008) Eddy current testing of metallic sheets with defects using force measurements. Serb J Electr Eng 5(1):11–20

Brauer H, Porzig K, Mengelkamp J, Carlstedt M, Ziolkowski M, Toepfer H (2014) Lorentz force eddy current testing: a novel NDE – technique. COMPEL 33(6):1965–1977

Brauer H, Gorges S, Ziolkowski M (2017) Bewegungsinduzierte Wirbelstrompruefung von Verbundmaterialien. In: Proceedings of the DGZfP- Jahrestagung, Koblenz, Germany, pp 1–8

Buffa A, Maday Y, Rapetti F (2000) Calculation of eddy currents in moving structures by a sliding mesh-finite element method. IEEE Trans Magn 36(4):1356–1359

Carlstedt M (2016) A contribution to the experimental validation in Lorentz force eddy current testing. Dissertation, Technische Universität Ilmenau, Ilmenau

Carlstedt M, Porzig K, Ziolkowski M, Uhlig RP, Brauer H, Toepfer H (2013) Comparison of Lorentz force eddy current testing and common eddy current testing – measurements and simulations. Stud Appl Electromag XVII 39(1):218–225

Carlstedt M, Porzig K, Uhlig RP, Zec M, Ziolkowski M, Brauer H (2014) Application of Lorentz force eddy current testing and eddy current testing on moving nonmagnetic conductors. Int J Appl Electromagn Mech 45(1):519–526

Chady T, Spychalski I (2017) Eddy current transducer with rotating permanent magnets. In: 22nd International Workshop on Electromagnetic Nondestructive Evaluation (ENDE 2017), Saclay, France, p 2

Chari MVK, Konrad A, Palmo MA, D'Angelo J (1990) Simulation analysis of magnetic sensor for nondestructive testing by boundary element method. IEEE Trans Magn 26(2):877–880

COMSOL Inc., Burlington. Comsol Multiphysics, 2018

Davat B, Ren Z, Lajoie-Mazenc M (1985) The movement in field modeling. IEEE Trans Magn 21(6):2296–2298

Dawes CJ, Thomas WM (1996) Friction stir process welds aluminum alloys. Weld J 75(3):41–45

Demenko A (1996) Movement simulation in finite element analysis of electric machine dynamics. IEEE Trans Magn 32(3):1553–1556

Donoso G, Ladera CL, Martín P (2011) Damped fall of magnets inside a conducting pipe. Am J Phys 79(2):193–200

dos Santos TG, Ramos PM, dos Santos Vilaca P (2008) Nondestructive testing of friction stir welding: comparison of planar eddy current probes. In: Proceedings of the 16th IMEKO TC4 Symposium, Florence, Italy, pp 507–512

Geirinhas Ramos HM, Rocha T, Pasadas D, A. Lopes Ribeiro (2013) Velocity induced eddy currents technique to inspect cracks in moving conducting media. In: IEEE International Instrumentation and Measurement Technology Conference (I2MTC) Proceedings, The Depot, Minneapolis, pp 931–934

German Institute for Standardization (2015) Ruehrreibschweißen – Aluminium – Teil 5: Qualitaets- und Pruefungsanforderungen. DIN EN ISO 25239-5

Golovanov C, Coulomb JL, Marechal Y, Meunier G (1998) 3D mesh connection techniques applied to movement simulation. IEEE Trans Magn 34(5):3359–3362

Gorges S, Brauer H, Ziolkowski M, Carlstedt M, Weise K, Schmidt R, Mengelkamp J (2016) Motion-induced eddy current testing of composite materials. In: Proceedings of the 19th World Conference on Non-destructive Testing (WCNDT), Munich, Germany, Fr.1.F

Haus H, Melcher JR (1989) Electromagnetic fields and energy. Prentice-Hall, Englewood Cliffs

Hellier CJ (2013) Handbook of nondestructive evaluation, 2nd edn. McGraw-Hill Education LLC, New York

Ida N (1995) Numerical modeling for non-destructive evaluation, 1st edn. Chapman & Hall, London

Ida N, Bastos JPA (1997) Electromagnetics and calculation of fields, 2nd edn. New York, NY, Springer

Jiles DC (1990) Review of magnetic methods for nondestructive evaluation (Part 2). NDT Int 23(2):83–92

Konstantin Weise (2016) Advanced modeling in Lorentz force eddy current testing. Dissertation, Technische Universität Ilmenau, Ilmenau

Kim YG, Fujii H, Tsumura T, Komazaki T, Nakata K (2006) Three defect types in friction stir welding of aluminum die casting alloy. Mater Sci Eng A Struct 415(1–2):250–254
Kirpo M, Tympel S, Boeck T, Krasnov D, Thess A (2011) Electromagnetic drag on a magnetic dipole near a translating conducting bar. J Appl Phys 109(11):113921
Lai HC, Rodger D, Leonard PJ (1991) A finite element method for problems with moving parts. In: Proceedings of 8th International Conference on Computation in Electromagnetics (CEM91), London, UK, pp 211–213
Leonard PJ, Lai HC, Hainsworth G, Rodger D, Eastham JF (1993) Analysis of the performance of tubular pulsed coil induction launchers. IEEE Trans Magn 29(1):686–690
Marechal Y, Meunier G, Coulomb JL, Magnin H (1992) A general purpose tool for restoring inter-element continuity. IEEE Trans Magn 28(2):1728–1731
ME-Meßsysteme (2014) Data sheet – K3D40. ME-Meßsysteme GmbH
Mengelkamp J (2016) Forward and inverse calculation methods for Lorentz force evaluation applied to laminated composites. Dissertation, Technische Universität Ilmenau, Ilmenau
Mengelkamp J, Ziolkowski M, Weise K, Carlstedt M, Brauer H (2015) Permanent magnet modeling for Lorentz force evaluation. IEEE Trans Magn 51(7):6301211
Mengelkamp J, Lattner D, Haueisen J, Carlstedt M, Weise K, Brauer H, Ziolkowski M, Eichardt R (2016) Lorentz force evaluation with differential evolution. IEEE Trans Magn 52(5):6001310
Mengelkamp J, Carlstedt M, Weise K, Ziolkowski M, Brauer H, Haueisen J (2017) Current density reconstructions for Lorentz force evaluation. Res Nondestruct Eval 28(2):76–100
Mishra RS, Ma ZY (2005) Friction stir welding and processing. Mater Sci Eng R Rep 50(1–2):1–78
Mishra RS, De PS, Kumar N (2014) Friction stir welding and processing: science and engineering. Springer International Publishing, Cham
Mook G, Hesse O, Uchanin V (2007) Deep penetrating eddy currents and probes. Materials Testing, 49(5):258–264
Mook G, Michel F, Simonin J (2011) Electromagnetic imaging using probe arrays. Strojniški vestnik 57(3):227–236
Muramatsu K, Nakata T, Takahashi N, Fujiwara K (1996) Linear AC steady- state eddy current analysis of high speed conductor using moving coordinate system. IEEE Trans Magn 32(3):749–752
Muramatsu K, Takahashi N, Hashio T, Yamada C, Ogawa M, Kobayashi S, Kuwahara T (1999) 3-D eddy current analysis in moving conductor of permanent magnet type of retarder using moving coordinate system. IEEE Trans Energy Convers 14(4):1312–1317
Ooi B-T (1977) A dynamic circuit theory of the repulsive magnetic levitation system. IEEE Trans Power Appar Syst 96(4):1094–1100
Ooi B-T, Jain OP (1979) Force transients at guideway butt joints in repulsive magnetic levitation system. IEEE Trans Power Appar Syst PAS-98(1):323–330
Petković B (2013) Assessment of linear inverse problems in magnetocardiography and Lorentz force eddy current testing. Dissertation, Technische Universität Ilmenau, Ilmenau
Petković B, Haueisen J, Zec M, Uhlig RP, Brauer H, Ziolkowski M (2013) Lorentz force evaluation: a new approximation method for defect reconstruction. NDT & E Int 59:57–67
Pietras A, Weglowski MS (2014) Imperfections in FSW joints and NDT methods of their detection. Biul Inst Spawalnictwa w Gliwicach 58(2):23–32
Pitkänen J, Haapalainen J, Lipponen A, Sarkimo M (2014) NDT of friction stir welding PLFW1 to PLFW5 (FSWL98, FSWL100, FSWL101, FSWL102, FSWL103) NDT Data Report
Porzig K, Carlstedt M, Ziolkowski M, Brauer H, Toepfer H (2014) Reverse engineering of ECT probes for nondestructive evaluation of moving conductors. AIP Conf Proc 1581:1519–1525
Preston TW, Reece ABJ, Sangha PS (1988) Induction motor analysis by time-stepping techniques. IEEE Trans Magn 24(1):471–474
Ramos HG, Lopes Ribeiro A (2014) Present and future impact of magnetic sensors in NDE. Procedia Eng 86(1):406–419
Ramos HG, Rocha T, Pasadas D, Ribeiro AL (2013) Faraday induction effect applied to the detection of defects in a moving plate. Rev Prog Q 32(1):1490–1497
Reddy NR, Reddy GM (2016) Friction stir welding of aluminium alloys – a review. Int J Mech Eng Technol 7(2):73–80

Reitz JR (1970) Forces on moving magnets due to eddy currents. J Appl Phys 41(5):2067–2071
Reitz JR, Davis LC (1972) Force on a rectangular coil moving above a conducting slab. J Appl Phys 43(4):1547–1553
Rocha TJ (2017) Velocity induced eddy current testing. Dissertation, Instituto Superior Te'cnico Lisboa, Lisboa
Rocha TJ, Ramos HG, Lopes Ribeiro A, Pasadas DJ, Angani CS (2015a) Studies to optimize the probe response for velocity induced eddy current testing in aluminium. Measurement 67(1):108–115
Rocha TJ, Ramos HG, Lopes Ribeiro A, Pasadas DJ (2015b) Magnetic sensors assessment in velocity induced eddy current testing. Sensors Actuators A Phys 228(1):55–61
Rodger D, Eastham J (1985) Characteristics of a linear induction tachometer – a 3D moving conductor eddy current problem. IEEE Trans Magn 21(6):2412–2415
Rodger D, Lai HC, Leonard PJ (1990) Coupled elements for problems involving movement (switched reluctance motor). IEEE Trans Magn 26(2):548–550
Rodger D, Leonard PJ, Eastham JF (1991) Modelling electromagnetic rail launchers at speed using 3D finite elements. IEEE Trans Magn 27(1):314–317
Roemer U, Schoeps S, Weiland T (2014) Approximation of moments for the nonlinear magnetoquasistatic problem with material uncertainties. IEEE Trans Magn 50(2):417–420
Rosado LS, Santos TG, Piedade M's, Ramos PM, Vilaça P (2010) Advanced technique for non-destructive testing of friction stir welding of metals. Measurement 43(8):1021–1030
Saslow WM (1992) Maxwell's theory of eddy currents in thin conducting sheets, and applications to electromagnetic shielding and MAGLEV. Am J Phys 60(8):693–711
Shi Y, Zhang C, Li R, Cai M, Jia G (2015) Theory and application of magnetic flux leakage pipeline detection. Sensors 15(12):31036–31055
Storn R, Price K (1997) Differential evolution – a simple and efficient heuristic for global optimization over continuous spaces. J Glob Optim 11(4):341–359
Tan Y, Wang X, Moreau R (2015) An innovative contactless method for detecting defects in electrical conductors by measuring a change in electromagnetic torque. Meas Sci Technol 26:035 602
TETRA Gesellschaft für Sensorik, Robotik und Automation mbH. Betriebsanleitung: BASALT-C MMP-15, 2015
Thess A, Votyakov E, Kolesnikov Y (2006) Lorentz force velocimetry. Phys Rev Lett 96(16):164501
Thess A, Votyakov E, Knaepen B, Zikanov O (2007) Theory of the Lorentz force flowmeter. New J Phys 9(8):299
Thomas WM, Nicholas ED, Needham JC, Murch MG, Temple-Smith P, Dawes CJ (1991) Friction stir butt welding. International Patent Application: PCT/GB92/02203
Trowbridge CW, Sykulski JK (2006) Some key developments in computational electromagnetics and their attribution. IEEE Trans Magn 42(4):503–508
Uhlig RP (2014) An experimental validation of Lorentz force eddy current testing. Universitätsverlag Ilmenau, Ilmenau
Uhlig RP, Zec M, Ziolkowski M, Brauer H (2011) Lorentz force eddy current testing: validation of numerical results. Proc Electrotech Inst 251:135–145
Uhlig RP, Zec M, Brauer H, Thess A (2012a) Lorentz force eddy current testing: a prototype model. J Nondestruct Eval 31(4):357–372
Uhlig RP, Zec M, Ziolkowski M, Brauer H, Thess A (2012b) Lorentz force sigmometry: a contactless method for electrical conductivity measurements. J Appl Phys 111(9):094914
Voellner G (2010) Rührreibschweißen mit Schwerlast-Industrierobotern. Forschungsberichte IWB. Herbert Utz Verlag, München
Weise K, Schmidt R, Carlstedt M, Ziolkowski M, Brauer H, Toepfer H (2015a) Optimal magnet design for Lorentz force eddy current testing. IEEE Trans Magn 51(9):6201415
Weise K, Ziolkowski M, Carlstedt M, Brauer H, Toepfer H (2015b) Oscillatory Motion of Permanent Magnets Above a Conducting Slab. IEEE Trans Magn 51(10):7209113

Yamazaki K (1997) Generalization of 3D eddy current analysis for moving conductors due to coordinate systems and gauge conditions. IEEE Trans Magn 33(2):1259–1262
Yamazaki K (1999) 3D eddy current formulation for moving conductors with variable velocity of coordinate system using edge finite elements. IEEE Trans Magn 35(3):1594–1597
Ying P, Jiangjun R, Zhang Y, Yan G (2007) A composite grid method for moving conductor eddy-current problem. IEEE Trans Magn 43(7):3259–3265
Zec M (2013) Theory and numerical modelling of Lorentz force eddy current testing. Dissertation, Technische Universität Ilmenau
Zec M, Uhlig RP, Ziolkowski M, Brauer H (2013) Finite element analysis of nondestructive testing eddy current problems with moving parts. IEEE Trans Magn 49(8):4785–4794
Zec M, Uhlig RP, Ziolkowski M, Brauer H (2014) Three-dimensional numerical investigations of Lorentz force eddy current testing. Stud Appl Electromagn XVI 38(1):83–93
Zec M, Uhlig RP, Ziolkowski M, Brauer H (2015) Differentieller sensor, Prüfsystem und Verfahren zur Detektion von Anomalien in elektrisch leitfähigen Materialien. Patent EP2893336 A1, Institut Dr. Foerster GmbH & Co. KG
Ziółkowski M (2015) Modern methods for selected electromagnetic field problems. Wydawnictwo Uczelniane Zachodniopomorskiego Uniwersytetu Technologicznego, Szczecin
Ziolkowski M, Brauer H (2010) Fast computation technique of forces acting on moving permanent magnet. IEEE Trans Magn 46(8):2927–2930